Precambrian Research 332 (2019) 105410

Contents lists available at ScienceDirect

Precambrian Research

journal homepage: www.elsevier.com/locate/precamres

New insights on the paleobiology, biostratigraphy and paleogeography of the pre-Sturtian microfossil index taxon *Cerebrosphaera*

Y. Cornet[a,*], C. François[a], P. Compère[b], Y. Callec[c], S. Roberty[d], J.C. Plumier[d], E.J. Javaux[a,*]

[a] Early Life Traces & Evolution-Astrobiology, UR Astrobiology, Department of Geology, University of Liège, Sart-Tilman 4000, Belgium
[b] Functional and Evolutionary Morphology, Department of Biology, Ecology and Evolution, FOCUS, and Cell of Aid for Research and Education in Microscopy (CAREM-ULiege), University of Liège, Sart-Tilman 4000, Belgium
[c] Bureau de Recherches Géologiques et Minières, 3 av. Claude Guillemin, BP 36009, F-45060 Orléans Cédex2, France
[d] Ecophysiology and Animal Physiology Laboratory, Department of Biology, Ecology and Evolution, INBIOS, University of Liège, Sart-Tilman 4000, Belgium

ARTICLE INFO

Keywords:
Neoproterozoic
Cerebrosphaera
Wall ultrastructure
Microspectroscopy
Eukaryotes
Biostratigraphy

ABSTRACT

Important biological and geological events occurred during the early to middle Neoproterozoic. Among diversifying eukaryotic assemblages, populations of *Cerebrosphaera*, a distinctive and robust organic-walled vesicular microfossil (acritarch), show restricted stratigraphic distribution in several late Tonian to early Cryogenian worldwide successions. Here, we report the first occurrence of this taxon in Africa, in the Bouenza Subgroup (Republic of the Congo), enlarging its paleogeographic distribution and biostratigraphic significance. We also attempt to determine its biological affinity, using a combined analytical approach on specimens from the Kanpa and Hussar formations, Australia, and from the Svanbergfjellet Formation, Spitsbergen. Morphological and quantitative analyses were performed using light microscopy and scanning electron microscopy. The analyses show fine-scale morphological details and a morphological continuum between the former species *Cerebrosphaera ananguae* and *Cerebrosphaera buickii*, confirming their synonymy as proposed by a recently revised taxonomy. These observations also highlighted the presence of a thin external envelope, previously reported but formerly described and illustrated here for the first time. The characteristics of this envelope, the large diameter range of the vesicles, and the absence of excystment structure, suggest that *Cerebrosphaera* was a metabolically active growing cell. Ultrastructural analyses performed with TEM revealed a complex multilayered wall ultrastructure. The molecular composition and thermal maturity of the organic walls were estimated using Infrared and Raman microspectroscopies. The wall of *Cerebrosphaera* has a highly aromatic composition with short/highly branched aliphatic chains. The complex morphology and wall ultrastructure, combined with the large size (not a criterion by itself) of *Cerebrosphaera,* confirm its eukaryotic nature. Comparison with strikingly similar modern analogues permits to suggest a possible affinity to stem metazoan eggs, based on morphology and ultrastructure, but the chemical composition is unlike known biopolymers. This hypothesis is also consistent with estimates from molecular clocks. If confirmed, our results would provide an older direct evidence for stem metazoans than the Cryogenian biomarker and Ediacaran body fossil records. Our study reveals that *Cerebrosphaera* populations are important for Neoproterozoic biostratigraphy, but also participated to the diversification of eukaryotes in worldwide connected oceans.

1. Introduction

Both the late Mesoproterozoic and the early Neoproterozoic are key Era for the development of complex life on Earth. The early and middle Neoproterozoic, which comprise respectively the Tonian (1000 to 720 Ma; Shields-Zhou et al., 2016) and the Cryogenian (720 to 635 Ma; Shields-Zhou et al., 2016) periods, show an increased diversification in the fossil record of eukaryotes (Cohen and Macdonald, 2015; Huntley et al., 2006; Knoll et al., 2006; Parfrey et al., 2011; Riedman and Sadler, 2017; Yang et al., 2016; Xiao and Tang, 2018). Recent discoveries of new diverse eukaryotic assemblages suggest that this diversification probably started earlier, in the Mesoproterozoic (Javaux, 2011; Loron et al., 2019a; Baludikay et al., 2018; Beghin et al., 2017; Javaux and Knoll, 2017). Several eukaryotic crown groups appeared in the Neoproterozoic, including Chlorophyta (Butterfield, 2004; Butterfield, et al., 1994), Arcellinida (Porter et al., 2003; Porter and Riedman,

* Corresponding authors.
E-mail addresses: ycornet@doct.uliege.be (Y. Cornet), ej.javaux@uliege.be (E.J. Javaux).

https://doi.org/10.1016/j.precamres.2019.105410
Received 12 December 2018; Received in revised form 26 April 2019; Accepted 8 August 2019
Available online 09 August 2019

2019), possible Ciliates and Foraminifera (Bosak et al., 2012), and the first biomineralized protists (Cohen et al., 2017, 2018). Rhodophyta appeared earlier, in the Mesoproterozoic (Butterfield et al., 2000; Bengtson et al., 2017 but see Gibson et al., 2018). Both molecular clocks (Erwin et al., 2011) and possible biomarkers of sponges (Love et al., 2009; but see Antcliffe, 2013, and reply by Love and Summons, 2015; Brocks et al., 2017; Zumberge et al., 2018) suggest a Cryogenian origin and later diversification of macroscopic metazoans in the Ediacaran (Bobrovskiy et al., 2018), although an earlier appearance in dysoxic environments is also envisaged (Hammerlund, 2018; Mills et al., 2018). The early and middle Neoproterozoic is also a time of major environmental changes with the break-up of the supercontinent Rodinia (Myers et al., 1996; Li et al., 2008; Evans, 2009), heterogeneous conditions in redox-stratified oceans (e.g. Diamond and Lyons, 2018; Lyons et al., 2014; Guilbaud et al., 2015) probably affecting productivity and nutrient availability (Anbar and Knoll, 2002), changes in the carbon cycle reflected by highly fluctuating carbon isotopic curves, including the Bitter Springs Anomaly (BSA; Halverson et al., 2005; MacDonald et al., 2010), and the Snowball Earth glaciations (Calver et al., 2004; Fanning and Link, 2004; Zhou et al., 2004; Eyles et al., 2007; Eyles, 2008; Hill et al., 2011),

In the early Neoproterozoic, populations of robust and distinctive organic-walled vesicular microfossils (acritarchs) called *Cerebrosphaera* are found worldwide in several successions. This genus is defined by its distinctive cerebroid wrinkles of the vesicle wall (Butterfield et al., 1994). Riedman and Porter (2016) recently revised its taxonomy, synonymizing the different species *Cerebrosphaera buickii* (Butterfield et al., 1994), *Cerebrosphaera ananguae* (Cotter, 1999) and *Cerebrosphaera? globosa* (Ogurtsova and Sergeev, 1989) to *Cerebrosphaera globosa*.

Cerebrosphaera is reported from a large number of different basins and formations across the world with similar ages comprised between ~792 and ~738 Ma (Riedman and Sadler, 2017). It occurs in the Ryssö, Draken and Svanbergfjellet formations, Svalbard, Norway (Knoll and Calder, 1983; Knoll et al., 1991; Butterfield et al., 1994); in the Visingsö Formation, Sweden (Moczydlowska et al., 2010); in Australia, in the Hussar, Kanpa and Pirrilyungka formations, Officer Basin (Cotter, 1999; Hill et al., 2000; Grey et al., 2011), in the Skilogalee Dolomite and the Anama Siltstone, Burra Group (Hill et al., 2000; Grey et al., 2011), and in the 'Finke Bedś, Amadeus Basin (Grey et al., 2011); in the Tanner, Carbon Canyon and Duppa members, Chuar Group, USA (Porter and Riedman, 2019); in the Chichkan Formation, Kazakhstan (Ogurtsova and Sergeev, 1989; Sergeev and Schopf, 2010); in the Kulady and Kastakh formations, Lena-Anabar Basin, Russia (Nagovitsin et al., 2015); and in the Gouhou Formation, China (Zang and Walter, 1992) (Fig. 1). In summary, *Cerebrosphaera* appears in the rock record during or after the Bitter Springs Anomaly (BSA, between 811.51 ± 0.25 Ma and 788.72 ± 0.24 Ma; Swanson-Hyssel et al., 2015) and disappears before the onset of the Sturtian Glaciation (Grey et al., 2011), which was dated at a maximal age of 746 ± 2 Ma by Halverson et al. (2005). The characteristic morphology and short stratigraphic distribution make this genus easily recognisable even when present in small fragments and an excellent biostratigraphic index fossil taxon for the late Tonian (Hill et al., 2000; Riedman and Sadler, 2017).

The eukaryotic nature of *Cerebrosphaera* has been suggested previously based on morphology and size, but no detailed analyses were performed to support this hypothesis. In this paper, we attempt to better characterize and constrain the biological identity of this emblematic microfossil using morphological, morphometric, microchemical and ultrastructural analyses of *Cerebrosphaera* specimens from Spitsbergen and Australia, where large populations of fossils are available for study. We also report for the first time the presence of *Cerebrosphaera* in Africa. The sample comes from the Bouenza Subgroup, Mayombe Group, West Congo Supergroup, Niari basin of the Republic of the Congo. This discovery strengthens the value of *Cerebrosphaera* as an index taxon for the late Tonian, with also implications for the Neoproterozoic stratigraphy and paleogeography of the Congo Craton. Finally, we test hypotheses of taxonomic identification by comparing with published and new data from modern and fossil potential analogues.

2. Material

2.1. Cerebrosphaera microfossils

2.1.1. Australian specimens

The Australian samples come from the Lancer 1 and Empress 1A drill cores, which intersect the Kanpa and Hussar formations, Supersequence 1 of the Officer Basin located in Western Australia (Fig. 1). These drill cores, stored in the Geological Service of Western Australia (GSWA; Perth), were sampled by E. Javaux in 2010 with help of K. Grey. The age of these formations is estimated probably between 785 and 760 Ma and certainly younger than 802 Ma, based on correlations with other sedimentary basins in Australia (Stevens et al., 1999). The sedimentology and paleoenvironmental interpretations of these two formations were described in detail by Stevens et al. (1999) based on the Empress 1A drill core and by Mory and Haines (2005) based on the Lancer 1 drill core. The Kanpa Formation records fluctuating paleoenvironments ranging from shallow-marine to sabkha settings, under oxidizing to slightly reducing conditions, with variable sea level and redox conditions through the whole Kanpa Formation. Sediments from the Hussar Formation were deposited in a shallow marine nearshore environment.

2.1.2. Spitsbergen specimens

Svalbard specimens come from the L-10 sample of the Neoproterozoic Lower Dolomite Member, Svanbergfjellet Formation of the Akademikerbreen Group, Spitsbergen (Butterfield et al., 1994) (Fig. 1). This Group was deposited on the East Greenland-East Svalbard platform, a passive margin associated with the dislocation of the Supercontinent Rodinia. The margin was later disturbed by the Caledonian Orogeny (Halverson et al., 2007). The age of the Svanbergfjellet Formation is principally based on biostratigraphy, indicating a late Tonian-early Cryogenian age (Butterfield et al., 1994), and on carbon isotopic chemostratigraphy, recording the Bitter Springs Anomaly recently well-constrained and correlated worldwide at ca. 811–789 Ma (Halverson et al., 2007; MacDonald et al., 2010; Swanson-Hyssel et al., 2015). The Svanbergfjellet Formation records different supratidal to subtidal environments (Butterfield et al., 1994). All the specimens were picked out of macerates by N. Butterfield in Cambridge University (UK).

2.1.3. Republic of the Congo specimens

The Bouenza Subgroup was sampled by Y. Callec (Bureau de Recherches Géologiques et Minières, France) in the Republic of the Congo (Congo-Brazzaville). Several whole specimens and fragments of *Cerebrosphaera* were discovered in one sample (SB0058B, SIBITI sheet 1/200.000, X = 13.76813, Y = -3.90239) of the Bz2 Formation, Bouenza Subgroup, Mayombe Group, in the lower part of the West Congo Supergroup (999–566 Ma; Tack et al., 2001, Frimmel et al., 2006), from the Niari basin (Fig. 1). They co-occur with other common Proterozoic microfossils, such as smooth-walled isolated (*Leiosphaeridia crassa)* or colonial *(Synsphaeridium)* sphaeromorphs, filamentous sheaths (*Siphonophycus spp*), and also fragments of perforated sheaths. The sample consists of grey-green micaceous silty shale fragments containing the compressed microfossils. The shale fragments are reworked and preserved within an unconsolidated black argillite matrix (with TOC between 0.53 and 0.22%). The Bouenza Subgroup is considered as correlative to the Louila Subgroup in the Mayombe belt in Gabon and in the Republic of the Congo (Thiéblemont et al., 2009; Fullgraf et al., 2015) and with the Haut-Shiloango Subgroup in the Democratic Republic of the Congo (Cahen, 1978; Delpomdor et al., 2014; Fernandez-Alonso et al., 2018). The Bouenza Subgroup is

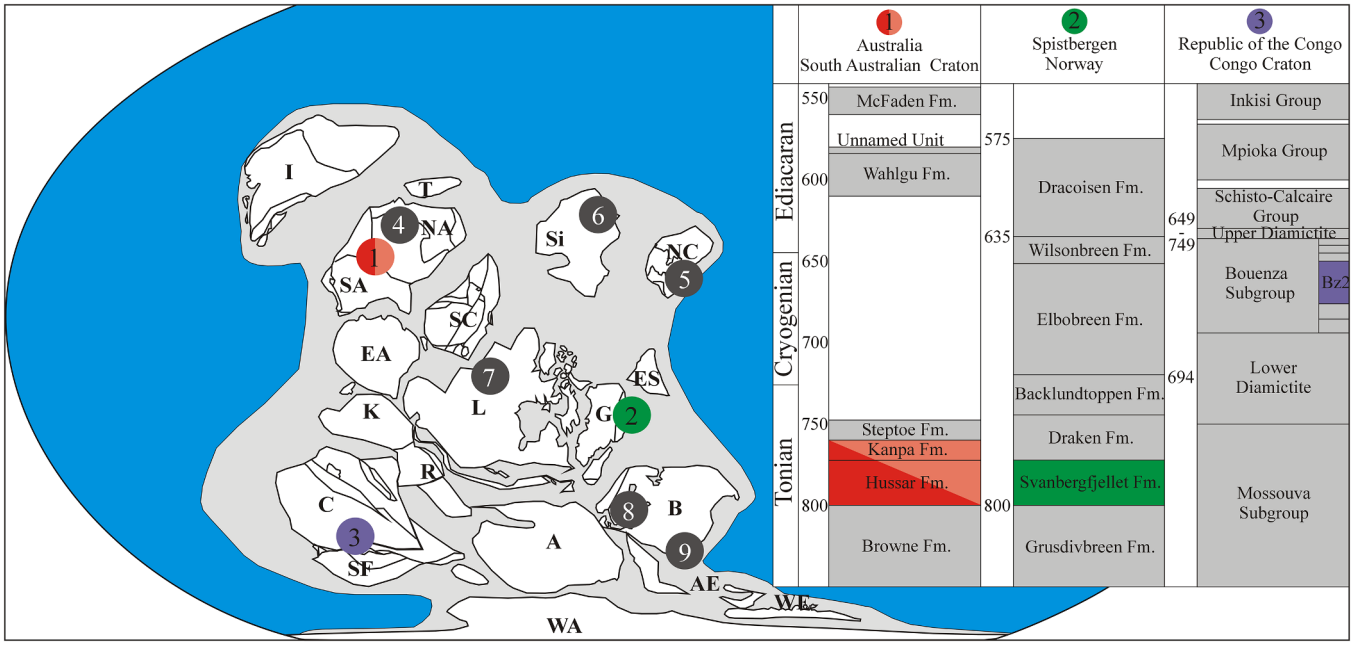

Fig. 1. Paleogeographic reconstitution of Rodinia at ~ 780 Ma showing the locations of fossiliferous sections and the specific units where *Cerebrosphaera* was identified and corresponding stratigraphic column for locations of this study. 1: South Australia, Officer Basin, Kanpa, Hussar and Pirrilyungka formations and Amadeus Basin, 'Finke' Beds. 2: Norway, Spitsbergen, Svanbergfjellet, Draken and Ryssö formations. 3: Republic of the Congo, Bouenza Subgroup, Bz2 Formation. 4: North Australia, Burra Group. 5: North China, Huaibei Group, Gouhou Formation. 6: Russia, Lena-Anabar Basin, Kulady and Kastakh Formations. 7: USA, Chuar Group, Tanner, Carbon Canyon, and Duppa members. 8: Sweden, Visingsö Group. 9: Kazakhstan, Maly Karoy Group, Chichkan Formation. Specific colour is assigned for each formation from this study. Red: Lancer 1 drill core; light red: Empress 1A drill core; Green: Svanbergfjellet Formation; Violet: Bz2 Formation. Abbreviations: A: Amazonia; A: Avalonia (East); Aw: Avalonia (West); B: Baltica; C: Congo; EA: East Antarctica; ES: East Svalbard; G: Greenland; I: India; K: Kalahari; L: Laurentia; NA: Northern Australia; NC: North China; R: Rio Plata; S: Sahara; SA: Southern Australia; SC: South China; Sf: Sao Francisco; Si: Siberia; T: Tarim; WA: West Africa. Modified from Li et al. (2013). (For interpretation of the references to colour in this figure legend, the reader is referred to the web version of this article.)

sandwiched between the lower diamictite and the Niari Group, also called the "Upper diamictite". It is divided into five different formations. The formations Bz0 to Bz3 are mostly siliciclastic while the formation Bz4 contains mostly oolithic and stromatolitic carbonates (Charles et al., 2015). In Gabon, rhyolitic tuffs intercalated into the Louila Subgroup yielded an U-Pb SHRIMP age of 713 ± 49 Ma (Thiéblemont et al., 2009) in agreement with the ca. 550–710 Ma detrital zircon age of the Sh6 unit of the Haut-Shiloango Subgroup in the Democratic Republic of the Congo (Frimmel et al., 2006), despite the low number of spot analysis (n = 7), the corresponding high value of discordance (up to 80%) and corresponding high error (± 20 to 557 Ma). The upper diamictite was dated using detrital zircons with ages ranging from 649 ± 40 to 769 ± 67 Ma (Affaton et al., 2015), consistent with the minimum U-Pb detrital zircon age of the Upper Diamictite at 707 ± 23 Ma (Straathof, 2011). The lower diamictite was dated using the U-Pb method on baddeleyite crystals from an intercalation of basalts and dolerites, which provided an age of 694 ± 4 Ma (Straathof, 2011). Detrital zircons from the top levels of the same lower Diamictite furnished a minimum age (U-Pb by LA-ICP-MS) of 678 ± 4 Ma (Archibald et al., 2018). These datings imply that the Bouenza Subgroup is younger than 694 Ma and probably older than the 635 Ma Marinoan glaciation (Frimmel et al., 2006; Tait et al., 2011).

2.2. Modern material

To decipher the identity of *Cerebrosphaera*, a broad literature survey of the morphology, ultrastructure and molecular structure of possible modern and fossil analogues of Proterozoic microfossils, such as bacteria, algae, other protists, and metazoan eggs, was carried out but revealed large gaps in knowledge. The cerebroid morphology of *Cerebrosphaera* is not reported in modern bacteria, algae or other protists, at our knowledge, but occurs in several arthropod eggs. Previous paleontological studies suggested a link between some spheroidal microfossils (acritarchs) and metazoan eggs based on morphology (Van Waveren, 1993; Xiao and Knoll, 2000) or morphology and ultrastructure (Cohen et al., 2009; Willman and Moczydlowska, 2007). Molecular phylogenies suggest their origins at least in the period between 850 and 635 Ma (Erwin et al., 2011). Therefore, to test the hypothesis of a possible metazoan affinity, microscopic and molecular analyses were performed on quiescent eggs and hatched eggs of the brine shrimp *Artemia salina*. *Artemia* eggs (Artemio Pur, JBL) were grown at 25 °C in a breeding container (Artemio 1, JBL) containing artificial seawater (salinity of 34; Reef Crystals, Aquatic systems, France) and eggs hatched within 48 h in the laboratory of Ecophysiology and animal physiology (Dr. S. Roberty, Prof. J.C. Plumier) of the University of Liège. This species was chosen as *Artemia* eggs are easily available commercially, and are commonly used as representative of other arthropod Anostrocan eggs in lab experiments. *Artemia* eggs are very resilient (can be stored several years), have smooth unornamented walls, hatch through a slit, and have a diameter ranging from 200 to 300 µm when dry (Wang and Sun, 2007) (Fig. 2). Branchiopoda Anostracan eggs can have cysts with a smooth surface, as in *Artemia*, or with a cerebroid surface, like in several other genera such as the 300–400 µm in diameter wrinkled cysts of *Branchinecta* or *Chirocephalus,* which have striking resemblance with *Cerebrosphaera* (see Figs. 1, 3 in Fanid et al., 2007). Several experimental taphonomic

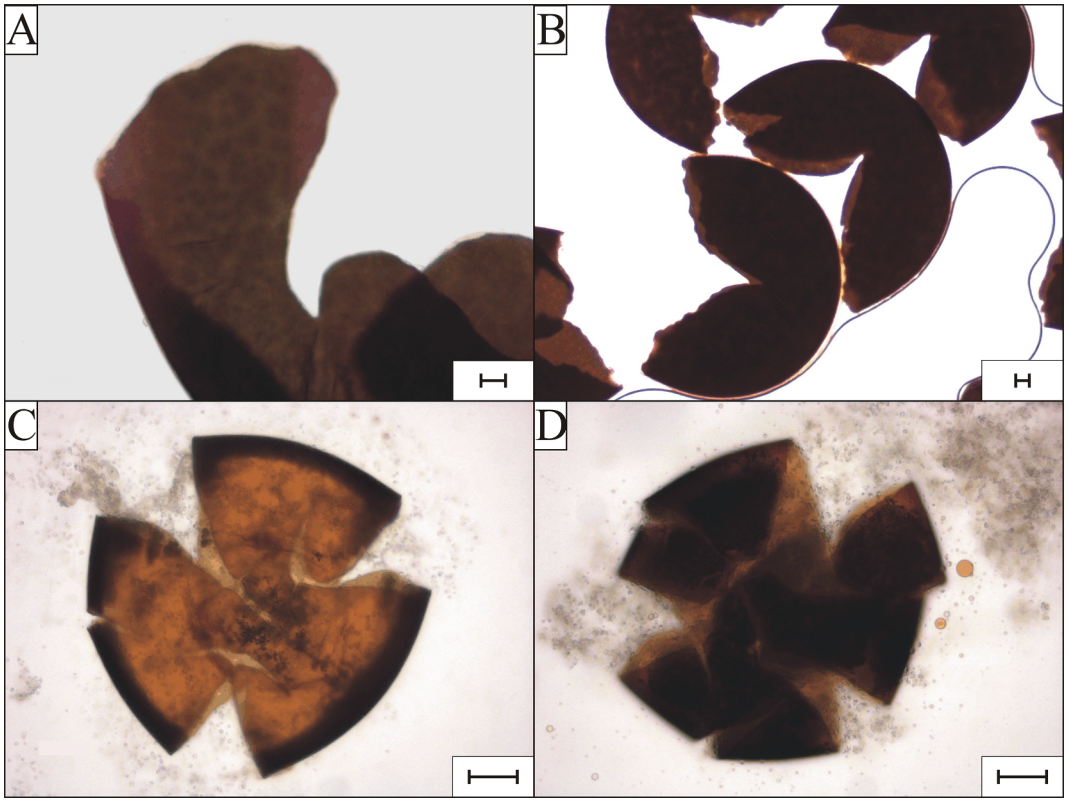

Fig. 2. Microphotographs of *Artemia* eggs. A, B: Compressed freshly hatched eggs showing a smooth surface and slight colour variations across the wall. C, D: compressed eggs, showing medial cracks due to the compression. Scale bar equal 50 μm.

studies showed that arthropod eggs can be preserved in the rock record (Martin et al., 2004; Martin et al., 2003; Raff et al., 2006; Pyle et al., 2006; Pan et al., 2015) and are common as organic-walled microfossils in modern sediments (van Waveren, 1993).

3. Methods

3.1. Sample preparation

3.1.1. Cerebrosphaera microfossils

Specimens from Australia and from the Republic of the Congo were prepared in the laboratory "Early Life Traces and Evolution-Astrobiology" (University of Liège, Belgium) using the static acid maceration method described in Grey (1999). Several microfossil slides were prepared from the kerogen macerates for morphological and morphometric analyses.

For the Kanpa and Hussar formations (Lancer 1 and Empress 1A drill cores), 221 specimens were observed in slides and photographed. For the Svanbergfjellet Formation, all specimens were initially extracted by N. Butterfield (U Cambridge, UK). Small portion of ~1 cm^3 of rocks were submerged with minimal agitation in HF concentrated at 48%. After digestion, the samples were rinsed with distilled water three times (Butterfield et al., 1994).

Specimens were individually handpicked under an inverted microscope using a micropipette and deposited or embedded on different types of support for observations with Environmental Scanning Electron Microscopy (ESEM), Scanning Electron Microscopy-Field Emission Gun (SEM-FEG) and Transmission Electron Microscopy (TEM), as well as analyses with Fourier Transform InfraRed (FTIR) and Raman microspectroscopies (Table 1).

3.1.2. Modern material

The morphology and wall ultrastructure of *Artemia* eggs are known (Anderson et al., 1970), but the wall composition has not been previously investigated with microspectroscopy. Here, we used freshly hatched eggs and unhatched eggs (10 specimens each), which were placed on ZnSe pastilles and dried for analyses with FTIR and Raman microspectroscopies.

3.2. Light microscopy

The diversity of the microfossil assemblages in the Kanpa and Hussar formations from the Lancer 1 and Empress 1A drill cores was studied by the observation of 52 palynological slides with a Zeiss Primo-star light microscope (Cornet, unpubl. MSc thesis), using descriptions available in the literature, especially Butterfield et al. (1994) for the Svanbergfjellet Formation, Cotter (1999) for the Supersequence 1 of the Officer Basin, and Hoffman and Jackson (1994) for the Bylot Supergroup, Canada. Microphotographs were taken with an Olympus BX51 coupled to an Olympus U-CMAD3 camera, and a Zeiss Axioimager equipped with the Axiovision software and a digital camera Axiocam MRc5, at the laboratory "Early Life Traces and Evolution-Astrobiology", University of Liège, Belgium. Morphometric analyses were done using the measurement tool of the Axiovision software at high magnification.

3.3. Scanning and environmental scanning electron microscopy (SEM and ESEM)

ESEM analyses of specimens mounted on glass slides using double-side carbon tape or aluminium tape, were performed on a FEI ESEM-FEG Philips XL-30, at the CAREM-ULiège (Cell of Aid for Research and Education in Microscopy). To obtain higher resolution imaging of the cerebroid wall and external envelope of *Cerebrosphaera,* specimens were deposited on ultra-flat 4″ Silicon Wafers and Au-coated with a Quorum Q150 ES metallizer for analyses with an Auriga 40 Field Emission Gun Scanning Electron Microscope (FEG SEM) Zeiss, at the electronic

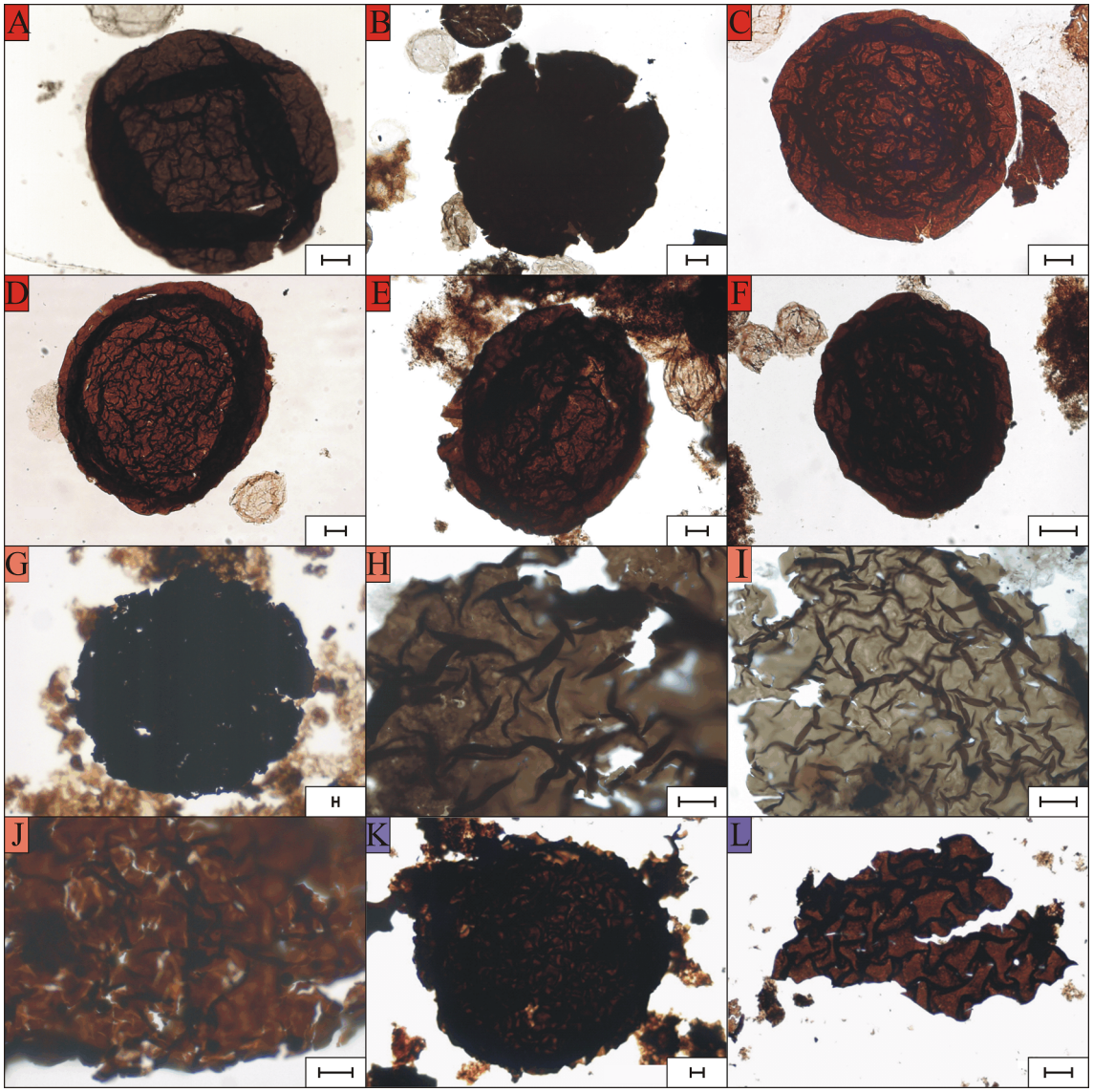

Fig. 3. Microphotographs of *Cerebrosphaera* specimens coming from different locations and depths. A-F: Lancer 1 drill core, Kanpa Formation, depth 680.10 m. Specimens showing different well-preserved specimens with colour ranging from dark brown to light brown. G-J: Empress 1A drill core, Kanpa Formation, depth 698.90 m G: heavily degraded but complete specimen H-J: magnifications of fragments of the wall showing the typical cerebroid folds of *Cerebrosphaera* allowing for an unambiguous identification. We can note the variation of the intensity of the colour of specimens coming from the same samples. K, L: Bz2 Formation. K: Entire vesicle showing the cerebroid folding of the wall. L: Vesicle fragment. Scale bar is 20 µm. *Cerebrosphaera* from the Svanbergfjellet formation are illustrated in Butterfield et al., 1994.

microscopy platform of the Institut Physique du Globe de Paris (platform PARI).

3.4. Transmission and scanning transmission electron microscopy (TEM and STEM)

For TEM and STEM observations, all specimens were first embedded in agar-agar gelose, then dehydrated in a graded ethanol series from 70% ethanol to 100% ethanol and then in 1,2-propylene oxide. The samples were finally infiltrated by epoxy resin, first in a 1:1 propylene oxide/epoxy resin melange and then in pure epoxy resin. Embedding of the specimens was made in silicon moulds to control specimen orientation and then left to polymerize at 60 °C for 3 days. The resin used is the hard mixture of AGAR Low Viscosity Resin kit (AGAR Scientific R10478).

Observations of the microfossil wall ultrastructure were performed on a TEM/STEM Tecnai G^2 Twin (CAREM-Uliège) working at 200 kV-accelerating voltage. Ultra-thin (60 and 100 nm-thick) transversal sections were made by a diamond knife on an ultramicrotome Reichert Ultracut E. They were put on formvar-coated copper grids (200 mesh) and observed in TEM and STEM-HAADF modes without chemical/heavy metal staining as it was shown unnecessary in previous studies (e.g. Javaux et al., 2004; Javaux et al., 2010).

3.5. Raman microspectroscopy

The analyses were performed on isolated specimens with a Renishaw INVIA Raman microspectrometer at the laboratory “Early Life Traces and Evolution-Astrobiology”, University of Liège, Belgium.

Raman analyses used an Ar-ion-40 mW monochromatic 514 nm laser source. Laser excitation was focused through a 50× objective to obtain a 1–2 µm spot size. Acquisitions of more than 10 spectra on each specimen were made in ‘Mapping point’-mode, with a 1800 L/mm grating. The Raman spectrum of each point was acquired in static mode

Table 1
Provenance and number of the specimens of *Cerebrosphaera* used for each type of analyses performed in the present study. The same specimens deposited on ZnSe pastille were used in Raman and FTIR microspectroscopy.

Provenance	Basin	Drill Core	Formation	Depth (m)	Morphometrics study (Light Microscopy)	SEM	Support	TEM	FTIR	Support	Raman	Support
Australia	Officer basin	Lancer 1	Kanpa	472.50	–	–	–	–	–	–	2	Glass slide
				666.37	54	–	–	–	–	–	–	–
				671.61	30	–	–	–	–	–	–	–
				675.30	34	–	–	–	–	–	–	–
				680.10	45	8	Carbon tape	5	17	ZnSe pastille	17	ZnSe pastille
						5	Aluminium tape				5	Glass slide
											1	Polished thin section
				682.88	53	3	silicon wafer	–	–	–	5	Glass slide
			Hussar	955.08	–	–	–	–	–	–	1	Glass slide
											2	Polished thin section
		Empress 1A	Kanpa	598.00	2	–	–	–	–	–	–	–
				698.90	6	–		1	7	ZnSe pastille	7	ZnSe pastille
				736.33	8	–	–	2	2	ZnSe pastille	2	ZnSe pastille
											6	Glass slide
			Hussar	1083.65	2	–	–	–	–	–		
				1097.80	2	–	–	–	–	–	3	Glass slide
				1099.00	2	–	–	–	–	–	1	Polished thin section
Svalbard	–	–	Svanbergfjellet	–	–	2	ZnSe pastille	6	2	ZnSe pastille	2	ZnSe pastille
						1	Carbon tape					

(fixed at 1150 cm^{-1}) for 1 × 1 s running time. This allowed the acquisition of Raman spectra with a 2000 cm^{-1} detection range and a 4 cm^{-1} spectral resolution. The software "Renishaw Wire 4.1" was used to process the spectral data. The baseline subtraction protocol was performed on a truncated spectrum between 1000 and 1800 cm^{-1}. The baseline was subtracted with a third order polynomial fit. Following this data processing, D1-, D2-, D3-, D4- and G-bands were fitted by a decomposition with the protocol described in Sforna *et al.* (2014).

As the Raman reflectance method appears to be a robust tool to evaluate the thermal maturity of poorly-organized carbonaceous material from Proterozoic rocks (see detailed methods and comparison of thermometers in Baludikay et al., 2018), this method was used in the present study.

For samples older than the Cambrian, due to the lack of the vitrinite precursor (higher land plants), the Raman reflectance parameter ($RmcR_0$ %), can be used as an equivalent of vitrinite reflectance *vR0%* (Liu et al., 2013; Sauerer et al., 2017). The $RmcR_0$ % uses the positions (ω) of the D1 and G peaks and is defined by:

$RmcR_0$ % ≡ *vR0 eq*% = 0.0537*(ωG–ωD1) − 11.21 (Liu et al., 2013).

This term can then be used in the following equation to calculate the temperature:

Tpeak burial (°C) = (ln (*vR0*%) + 1.68)/0.0124 (Barker and Pawlewicz, 1994).

Thermal maturity can also be estimated using the Thermal Alteration Index (TAI) which use the palynomorph wall colour and using the solid bitumen reflectance (*bR0%*) which is an equivalent to the *vR0%* (*vR0 eq*% = (*bR0*% + 0.41)/1.09).

Raman spectra were also compared here between extracted microfossils and microfossils *in situ* in polished thin sections of shales, to control the possible effect of acid attack during the maceration preparation on the wall molecular structure.

3.6. Fourier Transform InfraRed (FTIR) microspectroscopy

The analyses were performed with a Hyperion 2000 Bruker microscope coupled to a Tensor 27 FT-IR spectrometer at the Early Life Traces and Evolution-Astrobiology Laboratory, University of Liège, Belgium. Thirty-two scans were accumulated on each specimen and assembled into one spectrum covering a spectral domain between 400 cm^{-1} and 4000 cm^{-1}, with a resolution of 4 cm^{-1}. The spectra were treated with Opus 7.0 software. The atmospheric water and CO_2 were attenuated and the baseline was corrected.

Infrared spectroscopy allows the identification of the molecular structure of organic walls (carbon chain length, branching, presence of aliphatic, aromatic and other functional groups). Peak assignments are based on Larkin (2011) and on comparison with microfossil analyses in the literature (see Arouri et al., 1999; Coates, 2000; Marshall et al., 2005). The initial biopolymer composition of the living microorganisms can be altered by diagenesis (with possible aliphatization or sulfurization) and metamorphism (with possible aromatization) (Versteegh et al., 2012; Marshall and Marshall, 2015). Consequently, comparison is made between analyses of microfossils with the same taphonomic history (same sample, different taxa), between identical taxa from different context (different taphonomy), and control of maturity with Raman spectroscopy. Comparison with modern organisms permits, in some cases, to identify the microfossils, but is challenged by the lack of knowledge on the chemistry of preservable microscopic structures from modern prokaryotes and eukaryotes.

Band ratios can also be calculated to obtain quantitative characterization of the chemistry of the wall biopolymer. The CH_2/CH_3 ratio compares the intensity of the CH_2 antisymmetric stretching with the intensity of the CH_3 antisymmetric stretching. Its value can be directly linked to the length and degree of branching of the aliphatic chains of the biopolymer making up the wall of the microfossil vesicles. A high ratio reflects long and/or unbranched aliphatic chain, a low ratio is the sign of short and/or highly branched aliphatic chains (Lin and Ritz, 1993). To obtain the precise intensities needed for the calculation, the region comprised between 3000 and 2700 cm^{-1} was deconvoluted into five bands and fitted using the OPUS 7.0 software. The ~2955 cm^{-1} band is assigned to the antisymmetric CH_3 stretching, the ~2920 cm^{-1} band to the antisymmetric CH_2 stretching, the ~2890 cm^{-1} to the CH stretching, the ~2870 cm^{-1} band to the CH_3 symmetric stretching and the ~2850 cm^{-1} with the symmetric CH_2 stretching (Lin and Ritz, 1993; Marshall et al., 2005; Versteegh et al., 2007). The aliphatic/aromatic (Al/Ar) ratio allows quantifying the aromaticity of the biopolymer. It compares the intensity of the aliphatic hydrogen bonds of the 3000–2700 cm^{-1} region with intensity of the aromatic carbon bonds of the 1600 cm^{-1} band.

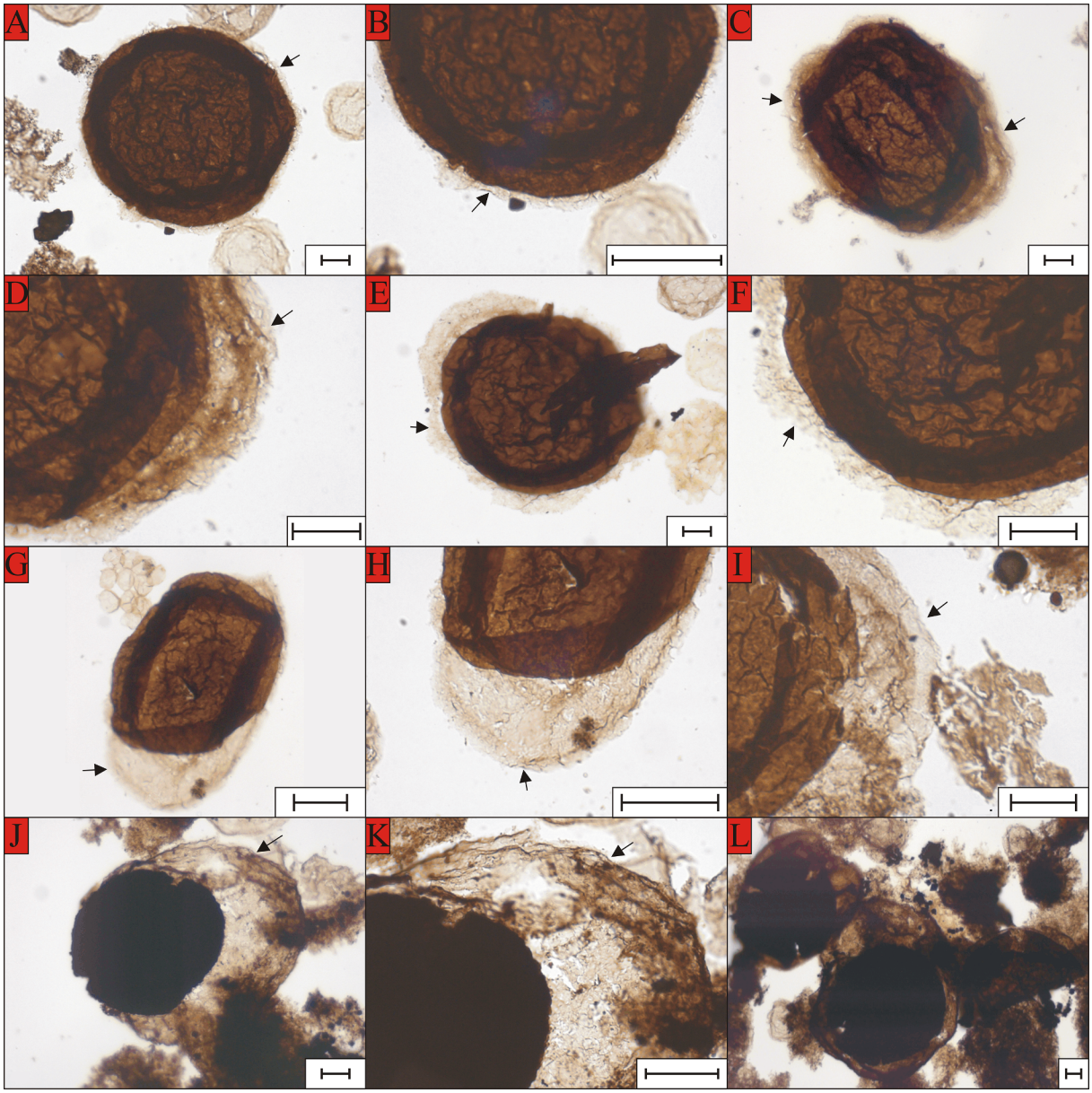

Fig. 4. Microphotographs of *Cerebrosphaera* specimens showing an envelope in variable state of preservation (black arrows), as a thin ripped rim attached to the vesicle (A-B) or whole and enclosing the vesicle (G-L). Scale = 20 µm. Black arrows: envelope. A, B: Kanpa Formation, depth 680.10 m. C, D: Kanpa Formation, depth 671.61 m. E-H: Kanpa Formation, depth 666.37 m. I-L: Kanpa Formation, depth 680.10 m.

4. Results

4.1. Morphology

The colour of *Cerebrosphaera* vesicles from Australia (Fig. 3) ranges from medium light brown to medium dark brown, corresponding to a Thermal Alteration Index (TAI) scale of 3− to 3 in the new TAI scale proposed by Baludikay et al. (2018), with about 20% of the specimens having opaque walls. The folds have a fairly regular distribution and morphology, although their widths vary among and across vesicles.

Some *Cerebrosphaera* vesicles are surrounded by an envelope, visible with light microscopy (Fig. 4), SEM and ESEM (Fig. 5). The envelope consists on a very thin, smooth and translucent membrane, preserved whole (Fig. 4G–L, Fig. 5A–E) or only as a thin shredded rim around the vesicles (Fig. 4A–F). Under ESEM and SEM, the wall appears slightly shagrinate and irregularly perforated (Fig. 5E). The wall ornamentation consist on 2 to 3 µm thick cerebroid wrinkles or folds fusing in triple point junctions (Fig. 5D–E), visible on both the inner and outer sides of the wall (Fig. 5F), and densely packed (Fig. 5G–H). The vesicle wall is locally degraded with tearing, holes, and mineral imprints (Fig. 5D–E). These irregular holes are not caused by predation.

The vesicle minimal diameter and the width of 10 folds regularly distributed among the vesicle surface were measured on 221 specimens from the Kanpa and Hussar formations. The studied specimens from the two other localities, Bouenza Subgroup and Svanbergfjellet Formation, have comparable size and morphologies (Table 2), but no envelope, although an envelope was mentioned in other material from the Svanbergfjellet Formation (Butterfield et al., 1994). There is no relationship between the mean width of the folds on the vesicle surface and the vesicle diameter, as confirmed by a correlation coefficient of 0.365 (Table 2, Fig. 6). When present, the preservation and size of the external envelope around the vesicles vary independently of both the vesicle size and the drill core depths (Table 2, Fig. 6).

The lack of correlation between the presence of an envelope and the vesicle diameter (Fig. 6) shows that it is not related to a developmental stage when vesicles reach a critical size. Rather, these observations

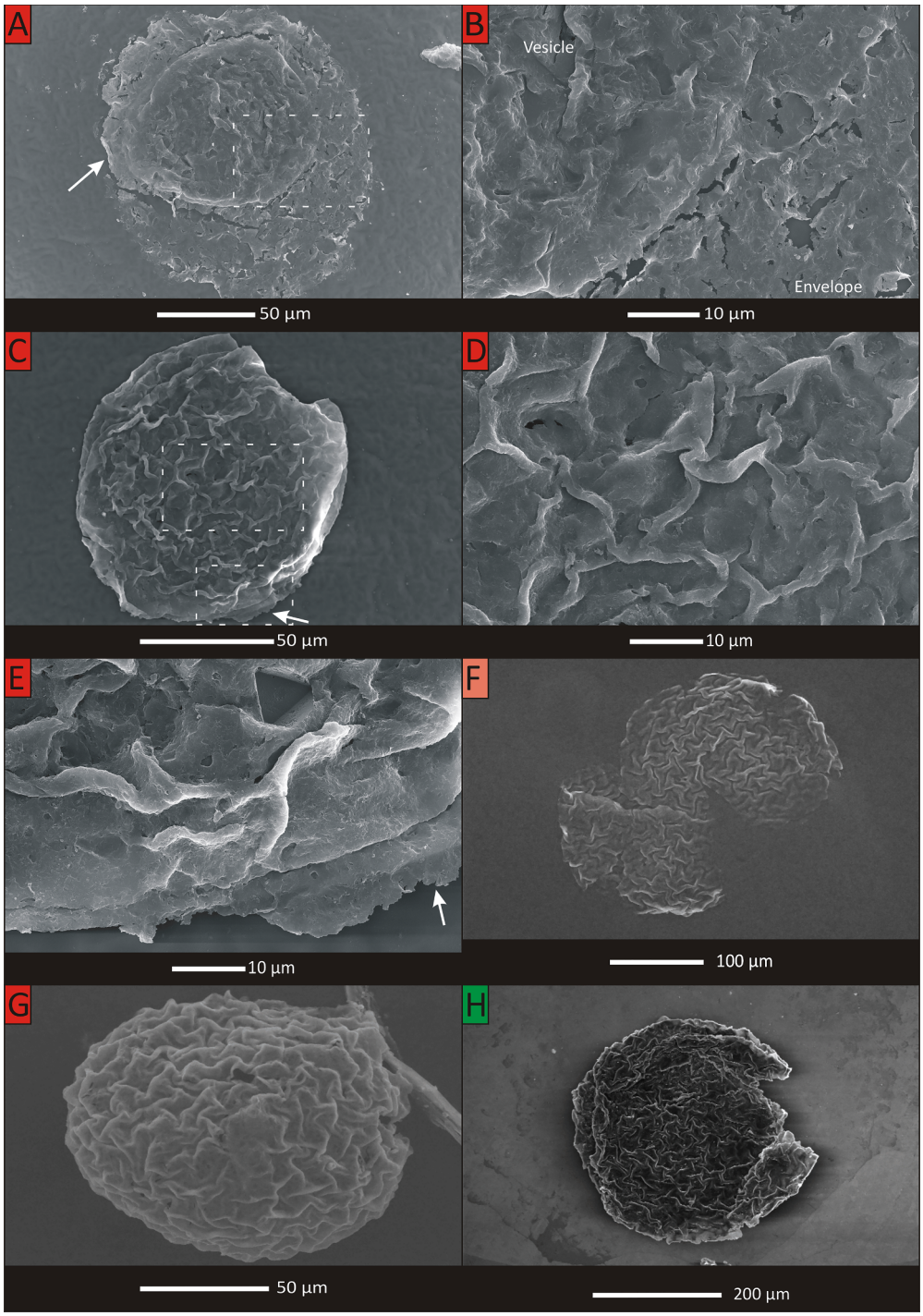

Fig. 5. SEM and ESEM images of *Cerebrosphaera*. A: Specimen from the Lancer 1 drill core, Kanpa Formation, depth 682.88 m showing a specimen with an envelope (arrow) (SEM, Au-coated, silicon wafers support, SE detector). B: details of the specimen in A showing the wrinkled vesicle and the thinner smooth envelope (SEM, Au-coated, silicon wafers support, SE detector). C: Specimen from Lancer 1 drill core, Kanpa Formation, depth 682.88 m showing a specimen with an envelope rim (arrow) (SEM, Au-coated, silicon wafers support, SE detector). D: Magnification of the specimen in C, showing details of cerebroid wrinkles. E: Magnification of the lower edge of the specimen in C showing the slightly degraded wall surface as well as a close view of the thin envelope rim visible at periphery (arrow). F: Specimen from the Empress 1A drill core, Kanpa Formation, depth 736.33 m showing the presence of cerebroid wrinkles on both the inner and outer sides of the wall of *Cerebrosphaera* (ESEM, carbon support, GSE detector). G: Specimen from the Lancer 1 drill core, Kanpa Formation, depth 680.10 m (ESEM, carbon support, GSE detector). H: Specimen of the Svanbergfjellet Formation (ESEM, Pt-coated, ZnSe pastille support, SE detector).

suggest that the envelope is part of the original morphology of *Cerebrosphaera*, but is variably preserved due to its lesser recalcitrance compared to the vesicle wall. The envelope is often irregularly opened, suggesting a taphonomic degradation rather than excystment. No excystment structures were observed on *Cerebrosphaera* vesicles nor on the envelope. They were also not previously reported in the literature.

The morphological observations, pattern of fold distribution on the vesicle surface, and the measurements of the vesicle diameters and cerebroid folds width on ~200 different specimens from the Kanpa and Hussar formations evidenced a morphological continuum within a single population. These morphometric and qualitative analyses support the taxonomic revision of the *Cerebrosphaera* species proposed by Porter and Riedman (2019).

4.2. Wall ultrastructure

TEM observations revealed two types of wall ultrastructures: a bi-layered and a tri-layered wall (Fig. 7). These two types occur among the *Cerebrosphaera* specimens from Australia, independently of the vesicle diameters. The specimens from Svalbard only show a bi-layered wall. The tri-layered wall ultrastructure (8 specimens studied) (Fig. 7A, B, C and D) exhibits a thin and electron-dense outer layer with a thickness ranging from 0.05 to 0.15 µm. This layer is frequently detached from the rest of the wall. The second intermediate layer is electron-dense with a porous texture. Its thickness is variable, ranging from 0.3 to 0.45 µm. The third and innermost layer is a homogeneous, electron-tenuous layer, with a thickness ranging from 0.40 to 0.50 µm. Local

Table 2
Morphometrics data obtained on *Cerebrosphaera*.

Origin	Basin	Drill core	Formation	Depth (m)	Number of vesicles	Minimal diameter (vesicle)	Width of the folds	Vesicle with an envelope	Minimal diameter (*Cerebrosphaera* in an envelope)	Minimal diameter (envelope)
Australia	Officer Basin	Lancer 1	Kanpa	666.37	54	Range : 55 to 650 µm	Mean:	14	Mean :	Mean :
				676.61	30	Mean:	1.9 ± 0.76 µm	5	165.65 ± 60 µm	182.15 ± 32 µm
				675.3	34	181.9 ± 83.89 µm	(N = 1730)	0	(N = 39)	(N = 39)
				680.1	45	(N = 240)		11		
				682.88	55			9		
		Empress 1A	Kanpa	598.00	2			0		
				698.90	6			0		
				736.33	8			0		
			Hussar	1083.65	2			0		
				1097.80	2			0		
				1099.00	2			0		
Africa	Bouenza	–	Bz2	–	4	Range : 100 to 360 µm		–	–	–
Svalbard	–	–	Svanbergfjellet	–	115	Range : 100 to 960 µm Mean: 365 ± 151 µm (Butterfield et al., 1994)		–	–	–

areas with heterogeneous textures are observed, randomly dispersed inside the wall (Fig. 6A and 6D). Thus, the total wall thickness ranges from 0.85 to 1 µm. Some dark material is often visible inside the vesicles, marking the position of the intracellular zone between compressed walls. The bi-layered ultrastructure (5 specimens studied) (Fig. 7E, F, G and H) includes a homogeneous electron-dense outer layer, with a thickness of 0.1 to 0.3 µm. It can easily detach from the rest of the wall or be lacking. The second inner layer is homogeneous and of medium electron-density, with a thickness of 1 to 2 µm. The layer seems relatively rigid as a high number of thin fractures perpendicular to the wall were observed.

Observations in STEM mode (Fig. 7B, F) reveal locally, small zones with heterogeneous textures, randomly distributed in the wall. These zones are brighter, indicating the presence of heavier elements. In some specimens, the intracellular space is really bright due to the probable presence of heavy elements and suggesting the presence of minerals, such as sulfide minerals like pyrites.

4.3. Thermal maturity and molecular structure of the wall biopolymer

4.3.1. Raman microspectroscopy

Raman microspectroscopy was used to estimate the thermal maturity of the *Cerebrosphaera* organic wall of specimens from the Kanpa, Hussar and Svanbergfjellet formations, and its possible effect on the chemical structure of the wall biopolymer and ultrastructure. Representative Raman spectra obtained on *Cerebrosphaera* specimens are visible on Fig. 8. Based on the spectral shape and on the literature (Schopf et al., 2005; Lahfid et al., 2010), the organic biopolymer making up the wall of the Australian specimens appears less mature than the wall of the Spitsbergen specimens (Fig. 8C). The organic matter consists of poorly ordered carbon with a D1-band higher than 100 cm^{-1} and an ID1/IG ratio lower than 1 (Table 3). These features, combined with differences of the FWHM-D1/FWHM-G ratio between the specimens from the minimal and maximal depths of the Lancer 1 and Empress 1A drill cores and the specimens of the Svanbergfjellet Formation indicate a higher maturity for the latter. The results are consistent with the expected thermal maturity of the samples based on their geological context and degree of metamorphism (Liu et al., 2013; Sauerer et al., 2017).

The spectral parameters allow to estimate the thermal maturity of the organic matter (Tables 3 and 4, methods detailed in Baludikay et al, 2018). In the Lancer 1 drill core, extracted specimens from 472.50, 680.10 and 955.08 m-depths show a mean temperature of 112 ± 15, 143 ± 15 and 136 ± 14 °C, respectively. In thin section, the specimens from 680 and 955 m depths show a mean temperature of 144 ± 14 and 163 ± 19 °C, respectively. For the Empress 1A drill core, the mean temperature is 148 ± 11 °C for the specimen at 736.33 m depth. For the specimens of the Svanbergfjellet Formation, the mean temperature is 197 ± 3 °C.

These temperatures are consistent, albeit slightly higher, with the TAI scale ranging from 3- to 3, estimated by microscopic observation of the microfossils wall colour, which corresponds to a temperature below 100 °C (Al-Ameri and Wicander, 2008). In addition, different measurements of the vR0 eq% exist for the Empress 1A drill core, (Kanpa Formation, depth between 516 and 830 m; Ghori in Stevens and Apak, 1999). These published values range from 0.52% to 1.00%, corresponding to a temperature varying between 82.7 and 135.5 °C.

4.3.2. FTIR microspectroscopy

Representative spectra obtained on isolated *Cerebrosphaera* specimens from the Kanpa and Hussar formations and the Svanbergfjellet Formation are shown on Fig. 9A, B and C, respectively. The detailed band assignation is visible on Table 5. For the Australian specimens, the more intense peak is due to stretching of the aromatic rings, centred at ~1610 cm^{-1}. Others peaks due to aromatic stretching are found near 1040 and 750 cm^{-1}. Secondary peaks are due to aliphatic CH_2, CH_3 and CH stretching in the region between 2970 and 2860 cm^{-1} and the region between 1450 and 1365 cm^{-1}.

The representative spectrum obtained from the Spitsbergen specimen (Fig. 9C) is similar, but varies slightly in intensity of some peaks, mainly the CH_2, CH_3 and terminal aromatic peaks. There are two weaker additional peaks, around ~2855 cm^{-1} due to an additional CH_3 stretching and at 1910 cm^{-1} due to stretching of the cumulated diene bond.

The representative spectrum obtained on *Artemia* egg (Fig. 9D) shows CH_2, CH_3 and CH stretching, absence of aromatic bonds, and several amide bonds characteristic of chitin and comparable to the band assignments of chitin standard by Ehrlich et al. (2013) shown in Table 5.

The CH_2/CH_3 ratios for the *Cerebrosphaera* specimens from Australia

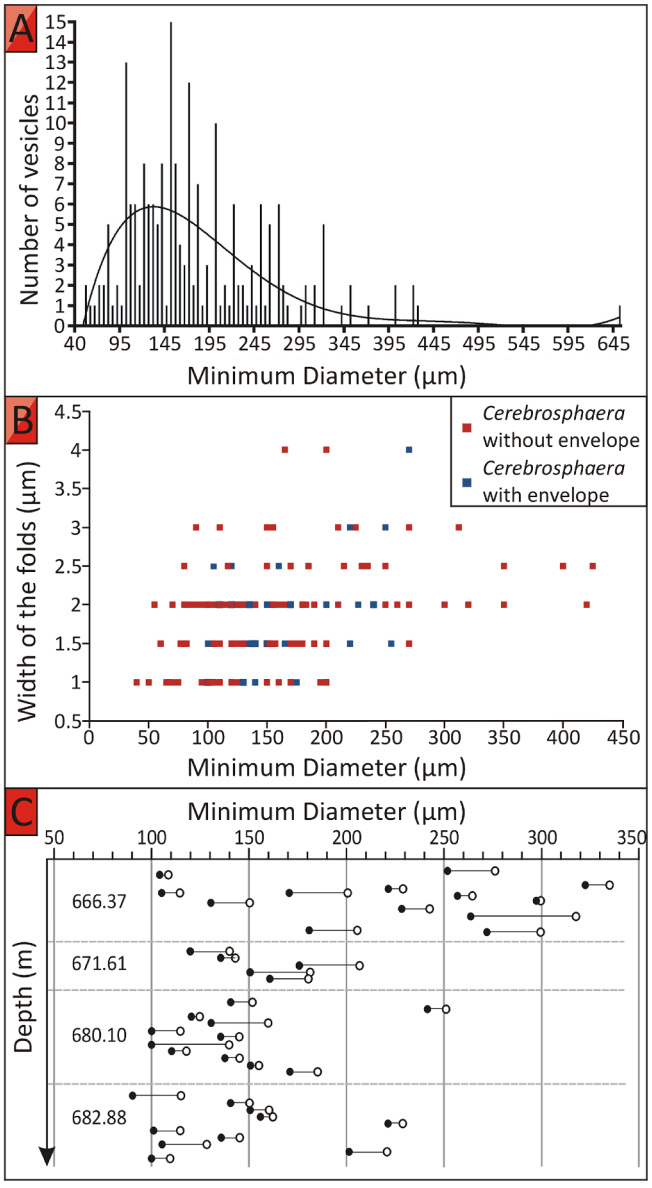

Fig. 6. Morphometry of *Cerebrosphaera* specimens. A: Size distribution of the fossil population observed in the Lancer 1 and Empress 1A drill cores. B: Distribution of the width of the folds compared to the vesicle diameter of the specimens with and without envelope. C: Size distribution of *Cerebrosphaera* vesicles in samples at different depths from the Lancer 1 drill core (black circles) and their respective envelope (white circles).

(Fig. 9A-C), range from 0.7 to 3.4 with a mean value of 2.2. These values indicate a biopolymer consisting of very short aliphatic chain, less than 10 carbons long, and with a probable size of 8 carbons (Lin and Ritz, 1993). The Al/Ar ratios range from 0.04 to 0.5 with a mean value of 0.1. The specimens of Spitsbergen showed, for the CH_2/CH_3 ratios, less dispersed values ranging from 2.0 to 2.5, also indicating a biopolymer consisting of very short aliphatic chains (Lin and Ritz, 1993). For the Al/Ar ratios, values range from 0.05 to 0.06, which is consistent with the higher aromaticity of the wall biopolymer when compared to the measurements obtained on the Australian specimens.

Thus, *Cerebrosphaera* vesicle walls are made of an aromatic biopolymer with short aliphatic chains (more aromatic in the Spitsbergen material due to its higher maturity), while *Artemia*'s eggs are made of chitin, a long N-rich polysaccharide chain (polymer of N-acetylglucosamine).

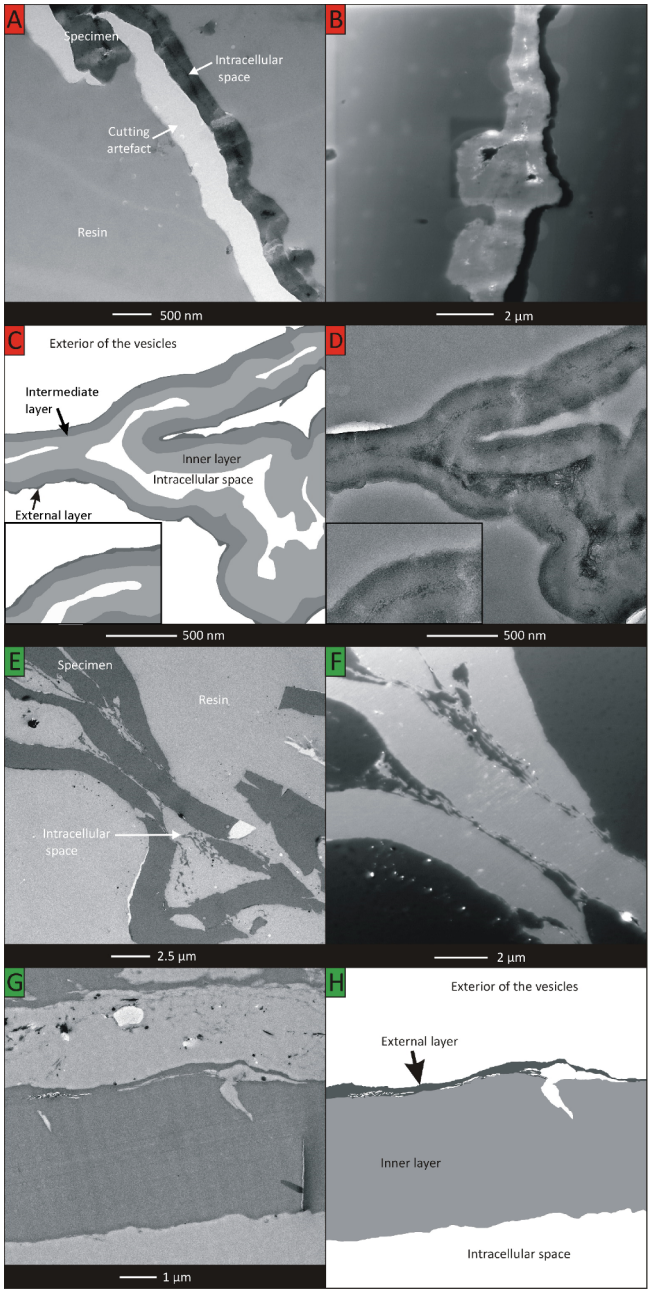

Fig. 7. Wall ultrastructure of *Cerebrosphaera*. A-D: specimens from the Lancer 1 drill core, Kanpa Formation, depth 680.10 m. Specimen showing a tri-layered wall ultrastructure of *Cerebrosphaera*. A: Low magnification TEM view of a specimen showing the folding of the compressed walls and the dark intracellular space (probably filled with minerals) in between. The very clear break is a sectioning artefact of the resin detaching from the microfossil. B: Low magnification STEM image showing the distribution of heavy elements in the wall. C, D: TEM detail and schematic views of the tri-layered ultrastructure showing a thin outer layer (arrow in C), an intermediate more porous layer (arrow in C) and an inner homogeneous layer. E-H: Specimens from the Svanbergfjellet Formation showing a bi-layered wall ultrastructure of *Cerebrosphaera*. E: Low magnification TEM view of a specimen of the Svanbergfjellet Formation showing the folding of the wall. All specimens of this Formation show a higher rigidity than the specimens coming from Australia, consistent with observations of fractures through the wall with light microscopy and with Raman analyses. F: Detailed STEM image showing the distribution of heavy elements (probable sulphide minerals) clustered in small structures (bright areas on the STEM image). G, H: TEM magnified and schematic views of a bilayered wall ultrastructure. The thin outer layer and the inner homogeneous layer are visible.

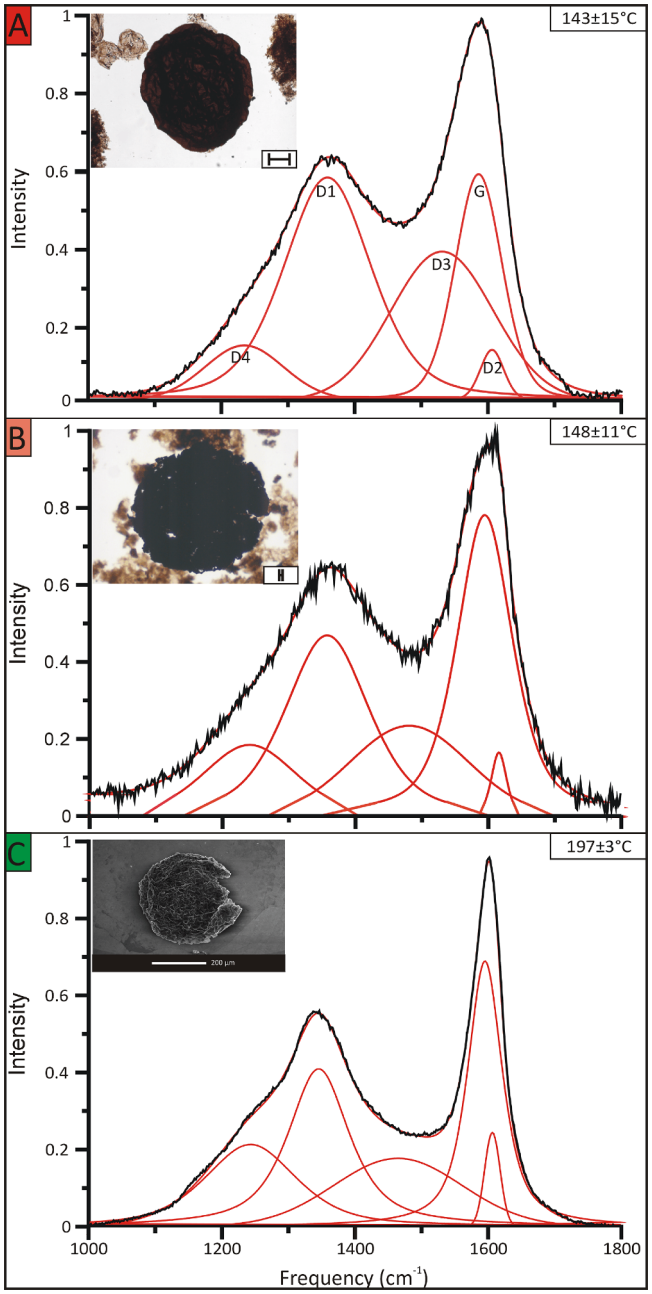

Fig. 8. Representative Raman spectra cut between 1000 and 1800 cm^{-1}, band deconvolution, and temperature estimates for specimens of *Cerebrosphaera*. A: from the Lancer 1 drill core, Kanpa Formation, depth 680.10 m B: from the Empress 1A drill core, Kanpa Formation, depth 736.33 m and C: from the Svanbergfjellet Formation.

5. Discussion

5.1. Eukaryoticity and paleobiology of Cerebrosphaera

The eukaryotic nature of *Cerebrosphaera* was previously suggested by several authors based on their ornamentation and large size (e.g., Sergeev and Schopf, 2010). A comparison with an algal cyst was also suggested based on the resemblance between the cerebroid folds and the crinkled wall of *Polygonium varium*, itself being inferred as the zygotic stage of chlorophycean algae (Moczydlowska, 2016). These studies were limited to morphological comparisons and did not investigate *Cerebrosphaera* morphometry, nor its wall ultrastructure and chemistry to support these hypotheses. Moreover, *Polygonium varium* is a crinkled vesicle within a process-bearing envelope, with a much smaller diameter (18 to 25 μm) and opening by medial split. Its putative algal affinity was proposed based on the morphology of its outer spiny envelope, a morphology known in some green algae but also other microorganisms. However, morphological convergence is possible, and at our knowledge, no extant green algae show the presence of true cerebroid folds. Thus *Cerebrosphaera* cannot be interpreted as algal based on morphological comparison with *Polygonium* which has a possible but unproven algal or other identity.

The term acritarch refers to an organic-walled hollow vesicle of unknown biological affinities (Evitt, 1963). However, a combination of morphological, ultrastructural and chemical analyses performed on these problematic microfossils and comparison with modern forms permits in some cases to identify them taxonomically, at the level of the domain or below (Arouri et al., 2002; Javaux and Marshal, 2006; Moczydlowska and Willman, 2009; Igisu et al., 2009; Moczydlowska et al., 2010; Willman and Cohen, 2011). Different characters can be used to recognize the eukaryotic nature of microfossils (Javaux et al., 2001, 2003, 2004; Knoll et al., 2006; Javaux and Knoll, 2017) including the presence of processes and ornamentation of the vesicle walls (Huntley et al., 2006; Talyzina and Moczydlowska, 2000), sometimes located on the inner surface of the vesicle (Javaux et al., 2004; Peng et al., 2009; Loron et al., 2019a), or structures making up the wall such as different types of plates (e.g. Javaux et al., 2004; Agić et al., 2015). The formation of both processes and ornamentations, the plastic morphology of some process-bearing acritarchs (e.g. *Tappania plana*, Javaux et al., 2001), and the presence of organic plates making up a wall, require the presence of an eukaryotic cytoskeleton (Cavalier-Smith, 2002), different from the bacterial cytoskeleton (Cabeen and Jacobs-Wagner, 2007). Another criterion is the complexity of the wall ultrastructure unknown in prokaryotes. However, many modern protists have uni-layered and unornamented walls, so their fossils are difficult to identify in the rock record without additional chemical or molecular analyses. Other eukaryotes show unique and taxonomically informative wall ultrastructures. Examples include the presence of pores and transverse canals in the thick uni-layered wall of prasinophyte phycoma (Wall, 1962; Jux 1969; Cohen et al., 2009; Moestrup et al., 2003; Arouri et al., 1999; Talyzina and Moczydlowska, 2000) or the trilaminar wall ultrastructure of some green algae (Atkinson et al., 1972; Pueschel et al., 1997; Hagen et al., 2002; Moczydlowska and Willman, 2009). Even when it is not possible to directly link a fossil with modern relatives, a complex ultrastructure may be unique to eukaryote when associated with other characters. This hypothesis is reinforced by the recalcitrant nature of the walls resisting acid maceration and presumably adverse conditions in nature, although not unique to eukaryotes (Javaux et al., 2004). Size is also not a discriminating criterion, since pico-eukaryotes (1–2 μm in diameter) and large prokaryotes (several 100's μm) do occur in nature (see review in Javaux et al., 2004), but is used in combination with complex morphology, wall ultrastructure and chemistry. Finally, the last criterion is the composition of the organic walls which may also be taxonomically informative. Many types of compounds are known and some can be linked directly with compounds found in modern eukaryotes, such as algaenan in a few green algae and dinoflagellates (Versteegh and Blokker, 2004; Marshall et al., 2005; De Leeuw et al., 2006; Kodner et al., 2008; Scholz et al., 2014), dinosporin in a few other dinoflagellates (Fensome et al., 1993; Head, 1996; Versteegh et al, 2012), chitin in some protists such as diatoms and ciliates (Foissner et al., 2005) and in various opisthokonts clades, including fungi and metazoans, and in algal clades (Muzzarelli, 1977; Schwelm et al., 2015), cellulose in oomycetes (Mélida et al., 2013), algae, and plants, and sporopollenin and lignin in plants (Graham and Wilcox, 2000; van Bergen et al., 2004). Experimental taphonomy can help determine the recalcitrance of modern organic-walled organisms (e.g. Graham et al., 2013, 2017). However, the composition and wall ultrastructure, or even the morphology of preservable structures of many modern organisms

Table 3
Average values of characteristic Raman parameters, Raman reflectance and Raman temperature. (N) = number of acquired spectra; (N′) = number of conserved spectra after initial assessment. See Baludikay et al., (2018) for explanation on methods and calculations. ωD1: position of the D1 band; ωG: position of the G band; FWHM-D1: full width at half maximum of the D1 band; FWHM-G: full width at half maximum of the G band; ID1: intensity of the D1 band; IG: intensity of the G band; RmcR0 %: Raman reflectance parameter.

Sampl	Location	Geological sequence	Formation	Drill core	Depth (m)	Rock type	Comment	Sample preparation
L1-472	Officer Basin	Supersequence 1	Kanpa	Lancer 1	472	Grey shale	*Cerebrosphaera buickii1*	Macerate
							Cerebrosphaera buickii2	Macerate
L1-680	Officer Basin	Supersequence 1	Kanpa	Lancer 1	680	Grey shale	*Cerebrosphaera buickii1*	Macerate
							Cerebrosphaera buickii2	Macerate
							Cerebrosphaera buickii3	Macerate
							Cerebrosphaera buickii4	Macerate
							Cerebrosphaera buickii1	Thin section
							Cerebrosphaera buickii2	Thin section
							Cerebrosphaera buickii3	Thin section
L1-955	Officer Basin	Supersequence 1	Kanpa	Lancer 1	955	Grey shale	*Cerebrosphaera buickii1*	Macerate
							Cerebrosphaera buickii2	Macerate
							Cerebrosphaera buickii1	Thin section
							Cerebrosphaera buickii2	Thin section
E1A-Cb3	Officer Basin	Supersequence 1	Kanpa	Empress 1A	736	Grey Shale	*Cerebrosphaera buickii1*	Macerate
L8 + L15	Spitsbergen		Svanbergfjellet	–	–	Shale	*Cerebrosphaera buickii1*	Macerate
							Cerebrosphaera buickii2	Macerate

N	N′	ωD1		ωG		ωG-ωD1		FWHM-D1		FWHM-G		FWHM-D1/FWHM-G	
		Mean	1σ	Mean	1σ	Mean	1σ	Mean	1σ	Mean	1σ	Mean	1σ
11	11	1355.7	3.3	1580.2	0.7	224.5	3.1	135.5	4.6	84.3	2.3	1.61	0.07
12	12	1358.7	1.6	1580.2	0.4	221.5	1.7	144.2	3.7	87.6	1.9	1.65	0.02
20	17	1351.7	3.4	1581.3	1.8	229.6	2.7	137.3	9.1	79.6	3.4	1.73	0.15
20	19	1349.4	2.0	1581.0	1.5	231.6	2.5	141.2	11.4	77.9	1.9	1.81	0.13
20	17	1349.6	3.3	1581.1	1.2	231.5	4.2	147.2	10.8	77.6	2.2	1.90	0.12
20	19	1354.5	2.0	1580.4	0.8	225.9	2.4	129.2	3.2	78.1	2.6	1.66	0.05
8	7	1359.6	0.8	1589.5	3.3	230.0	3.7	133.3	6.6	80.7	3.0	1.65	0.03
20	16	1359.7	0.6	1589.3	3.9	229.6	4.3	136.5	11.2	81.6	4.8	1.67	0.06
20	14	1359.4	1.2	1589.0	3.5	229.6	3.3	135.5	6.5	80.0	3.9	1.70	0.08
20	17	1354.4	3.2	1582.1	2.4	227.7	3.4	133.6	6.3	78.5	4.0	1.70	0.11
20	17	1355.9	3.7	1583.5	4.2	227.6	3.1	138.1	7.3	89.0	6.0	1.55	0.09
20	20	1355.1	3.7	1593.0	3.0	237.9	5.1	139.4	5.4	86.1	3.7	1.62	0.08
20	20	1354.2	3.9	1587.6	2.9	233.4	6.1	142.6	10.3	81.2	3.9	1.76	0.07
9	7	1359.2	3.7	1589.9	3.6	230.7	4.4	140.9	7.9	86.2	4.1	1.63	0.04
14	10	1349.8	0.7	1597.3	0.8	247.6	0.7	107.8	0.8	48.0	1.0	2.24	0.04
14	9	1348.6	0.7	1597.0	0.6	248.4	0.4	110.5	0.6	51.6	1.1	2.141	0.04

ID1		IG		ID1/IG		$RmcR_O$ %		T ($RmcR_O$ %) (°C)	
Mean	1σ	Mean	1σ	Mean	1σ	Mean	1σ	Mean	1σ
1181.6	118.9	1526.0	144.2	0.78	0.06	0.85	0.17	121	15
1387.0	102.8	1822.1	154.6	0.76	0.03	0.68	0.09	104	10
727.7	161.7	1022.9	210.8	0.71	0.07	1.12	0.15	144	10
1265.8	231.1	1631.7	272.0	0.78	0.07	1.23	0.14	151	9
1244.2	177.2	1610.3	203.2	0.77	0.06	1.22	0.23	150	16
870.6	430.4	1194.3	538.6	0.72	0.03	0.92	0.13	128	10
4473.5	1125.3	6096.6	1857.7	0.75	0.07	1.14	0.20	145	14
4170.4	1650.6	5831.3	2627.7	0.73	0.06	1.12	0.23	143	16
5520.4	1577.3	6962.8	2621.7	0.82	0.09	1.12	0.18	144	12
1073.5	315.5	1273.4	339.2	0.84	0.08	1.02	0.18	136	14
574.2	122.6	756.0	155.6	0.76	0.09	1.01	0.17	135	14
24621.5	3363.3	34098.1	4483.3	0.72	0.07	1.57	0.27	170	15
23307.1	3731.2	24592.7	5970.0	0.96	0.09	1.32	0.33	156	20
5805.0	1388.7	7486.8	2154.2	0.79	0.09	1.18	0.14	148	11
14955.3	916.4	35443.8	2334.5	0.42	0.01	2.08	0.04	195	1.4
12273.1	1214.5	27240.0	2735.7	0.45	0.00	2.13	0.02	196	0.7

are still uncharacterized.

The combined analyses performed on *Cerebrosphaera* specimens in this study permit several observations. The cerebroid folds with triple point junctions occur in compressed and three-dimensionally preserved specimens of *Cerebrosphaera* (Sergeev and Schopf, 2010; Porter and Riedman, 2016), suggesting they are a real surface ornamentation and not a taphonomic feature.

No excystment structure has been observed in the present and previous studies of *Cerebrosphaera* (Fig. 5I). This probably suggests that *Cerebrosphaera* is not a cyst. Moreover, the envelope shows a lesser resistance than the vesicle cell embodied within it, suggesting again that it is not a cyst wall. In addition, its large range of diameters suggests a metabolically active cell or a developing egg, rather than an inert cyst. Only in rare cases, such as for prasinophyte phycoma, the asexual cyst (Graham and Wilcox, 2000) is continually growing (Colbath, 1983; Knoll et al., 1991). The complex morphology of the microfossil is associated with a multi-layered wall ultrastructure. The thickness, texture, electron density and behaviour (detachment) of the different composing layers described here seem unique to *Cerebrosphaera* and differ from the ultrastructures described so far in the

Table 4
Compilation of mean temperatures calculated from Raman spectral parameters. See Table 3 for sample information.

Sample	Sample preparation	ωG-ωD1		*RmcR$_0$* %		*Tpeak* from *RmcR$_0$* % (°C)	
		Mean	1σ	Mean	1σ	Mean	1σ
L1-472	Macerate	222.9	2.9	0.76	0.15	112	15
L1-680	Macerate	229.6	3.8	1.12	0.20	143	15
	Thin section	229.7	3.8	1.12	0.20	144	14
L1-955	Macerate	227.7	3.2	1.01	3.25	136	14
	Thin section	235.7	6.01	1.44	0.32	163	19
E1A-Cb3	Macerate	230.7	4.4	1.18	0.14	148	11
L8-L15	Macerate	248.0	0.5	2.11	0.03	195	1.4

acritarch literature (e.g. Talyzyna, 2000; Talyzyna and Moczydlowska, 2000; Javaux et al., 2004; Peng et al., 2009; Agić et al., 2015). Hypotheses can be formulated regarding the presence of two types of wall ultrastructures. One is the existence of two different types of vesicles, exhibiting a different ultrastructure but similar morphology and chemistry. A second explanation is the existence of growing stages with different ultrastructures. However, it can be refuted by the absence of size differences between the bi- and tri-layered vesicles. A third possible explanation might lie in the differences in taphonomy and the state of preservation of the wall ultrastructure, the intermediate porous layer of tri-layered walls being either better preserved or a degraded part of the wall. The Australian specimens come from drill cores with well-preserved (non-metamorphosed) sedimentary rocks hosting relatively immature kerogen including acritarchs. It is unlikely that these acritarchs have been significantly altered, especially the robust *Cerebrosphaera* specimens. Specimens from Svalbard, showing only bi-layered structures, have undergone a higher degree of thermal maturity than the Australian specimens due to their geological history. Thus, the differences in the wall ultrastructure of the various specimens may be linked to the differential preservation of originally tri-layered walls.

In summary, *Cerebrosphaera* microfossils associate a typical cerebroid surface ornamentation, occurring both in compressed and three-dimensionally specimens, the presence of an envelope, a complex multi-layered wall made of a resistant biopolymer consisting of a resilient and mainly aromatic material with short aliphatic chains, and a large and variable size. This combination supports the hypothesis that these microfossils are affiliated to the domain Eukaryota and permits to test hypotheses regarding their taxonomy. No prokaryotes are known for having such combination of ornamentation, large size, complex wall ultrastructure(s) and acid-resistant walls, at our knowledge (Javaux et al., 2003).

5.2. Biological affinities of Cerebrosphaera

Cerebrosphaera can be compared to modern analogues and other microfossils using a set of characteristics that include the diameter, morphology, ultrastructure, opening structure if present, and chemistry. This approach of combining morphology and ultrastructure has been used previously to identify possible metazoan eggs (Cohen et al., 2009; Willman, 2009) or algae (Moczydlowska and Willman, 2009) among large Ediacaran acritarchs. However, combining morphology and ultrastructure with chemical analyses of microfossils (e.g Javaux and Marshal, 2006), is rarely used in other studies.

5.2.1. Morphology

The morphology of *Cerebrosphaera* is, to date, unique among known organic-walled microfossils. However, some other microfossils show a similar morphology with look-alike cerebroid folds (ridges and wrinkles). The ca. 635–551 Ma phosphorites of the Doushantuo Formation at the Weng'an section and in the Yangtze Gorges, South China, preserve population of *Megasphaera*, interpreted as phosphatized animal egg cell encapsulated within an egg envelope (Xiao et al., 2007; Xiao and Schiffbauer, 2009). This 400 to 1100 µm in diameter microfossil consists of one internal body encapsulated by a clearly demarcated envelope (Xiao and Knoll, 2000). The species *M. ornata* possesses an ornamented envelope with five different morphotypes (Xiao and Knoll, 2000), one of them resembling *Cerebrosphaera* with wider folds. Another unnamed phosphatized microfossil from the upper Cambrian Shenjiawan Formation, Wa'ergang sections, Hunan, China shows close resemblance with *Cerebrosphaera*, with a diameter of ca. 420 µm and cerebroid wrinkles with a distribution and a size compatible with those of *Cerebrosphaera* (Dong, 2009, Fig. 7).

Among possible modern analogues, to our knowledge, no known alga nor other protist show a comparable morphology to *Cerebrosphaera*. The only organisms with similar cerebroid ornamentation of the wall are various types of invertebrate eggs of the crustacean clade. The lobsters *Homarus gammarus* and *Nephrops norvegicus* have eggs with a wrinkled outer surface with triple point junction after suffering anoxic conditions during controlled decay experimentation (Martin et al., 2003; Martin et al., 2005). Several species, but not all, of the branchiopod *Eubranchipus* also show a cerebroid wrinkled surface (Xiao and Knoll, 2000; Belk et al., 1998), with similar size and fold arrangement (*E. holmanii* and *E. moorei*) or with smaller less pronounced folds (*E. intricatus*), or with wider and tighter packed cerebroid folds (*E. vernalis* and *E. neglectus*). Eggs of the branchiopod *Chirocephalus skorikowi* have a comparable size and cerebroid folds, but the folds are wider than those of *Cerebrosphaera,* while the other species do not show a cerebroid aspect (Mura, 2001). The eggs of the copepods *Eurytemora americana* (during the periods of peak population growth) (Berasategui et al., 2012), the diapause eggs of *Hemidiaptomus amblyodon* (Samchyshyna and Santer, 2010) or the various types of copepods eggs classed as "cerebrate-type" by Van Waveren (1993) all show a cerebroid external appearance (Table 6). The size of these eggs are similar to *Cerebrosphaera,* ranging from 55 µm to 650 µm (mean = 182 µm ± 84 µm, N = 209) (Table 6). It varies within the different considered class, genus and species but can also vary with environmental conditions such as the water temperature (Lonsdale and Levinton 1985). Branchiopoda Anostracan eggs can have cysts with a smooth surface, as in *Artemia eggs*, or with a cerebroid surface, like in several other genera such as the 300–400 µm in diameter wrinkled cysts of *Branchinecta* or *Chirocephalus,* which have striking resemblance with *Cerebrosphaera* (see Figs. 1, 3 in Fanid et al., 2007). Interestingly, such cysts with wrinkled surfaces are produced to survive in dry periods, and may protect the fairy shrimp embryo against stressful conditions such as salinity, temperature, predators or temporary desiccation in vernal pools (Fanid et al., 2007). The eggs of other early-diverging metazoans such as sponges, placozoa and cnidaria, appear to have a simple morphology showing no cerebroid folding (Table 6). Their sizes are in the lower range of *Cerebrosphaera*'s diameter (Table 6).

5.2.2. Wall ultrastructure of Cerebrosphaera

The wall ultrastructure of *Cerebrosphaera* is complex, with two or three different layers. The comparison with the wall ultrastructure of modern organisms' cyst or eggs is hampered by the limited number of studies (summarizes in Table 6). Modern copepod eggs tend to show a recurring pattern: simple unilayered subitaneous eggs and more complex and resistant diapause eggs showing the presence of multiple layers of the wall ultrastructure (Santella and Ianora, 1990; Ianora and Santella, 1991; Couch et al., 2001; Samchyshyna and Santer, 2010; Berasategui et al., 2012). Early-diverging metazoans like sponges have different means of reproduction, some genera being viviparous (Ereskovsky, 2000) while other are oviparous (Mariani et al., 2000). The sponge oocytes vary greatly in morphology, size and structure according to the species but most of them tend to have a thin wall ultrastructure composed of multiple very thin organic layers (Simpson, 1984; Riesgo and Maldonado, 2009). However, some sponges are known to form dormancy structure called gemmule, to withstand harsh

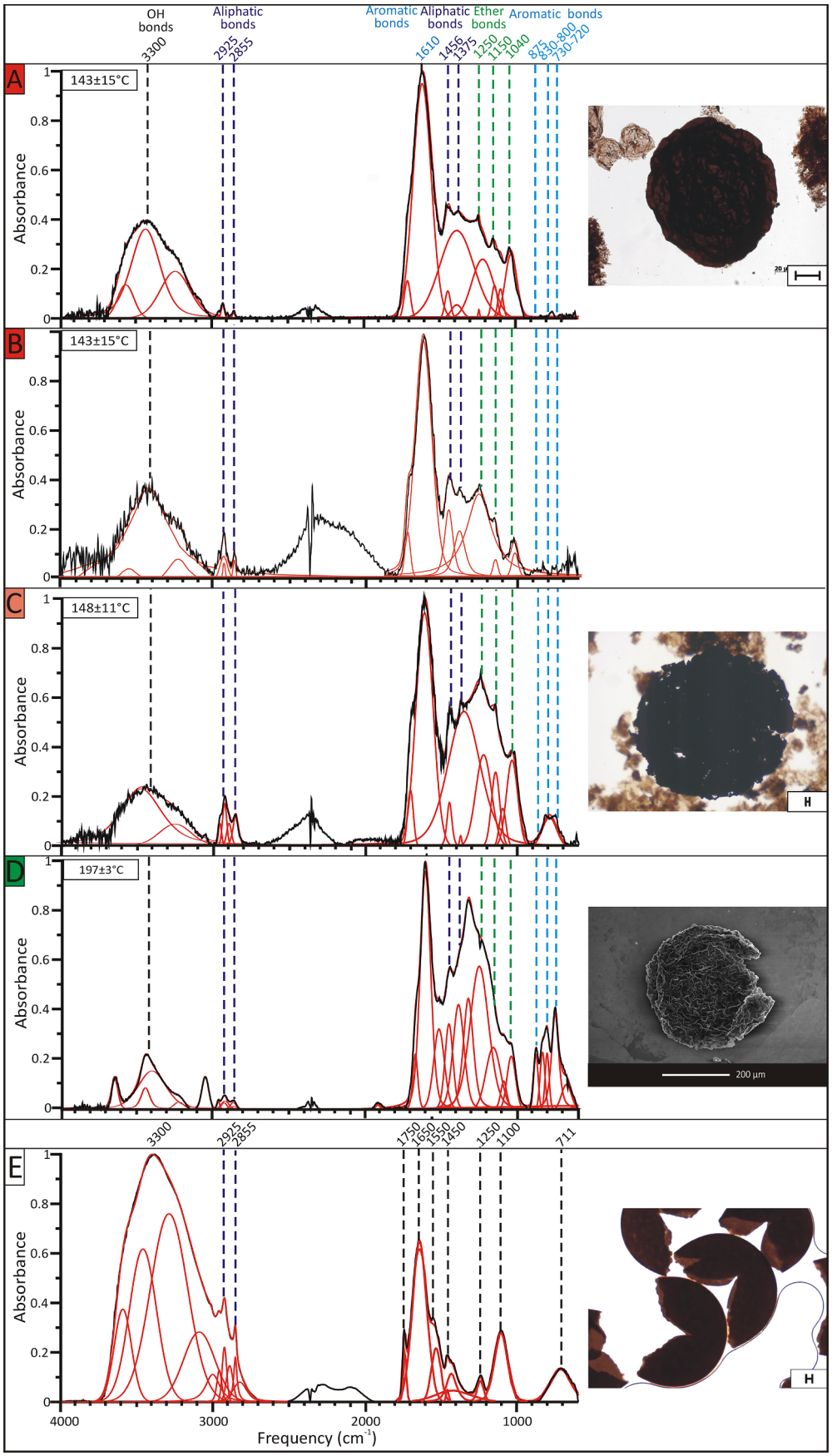

Fig. 9. Representative FTIR spectra (baseline, atmospheric water and CO_2 and ZnSe substracted) and associated deconvolution for band assignation. A, B: specimens of *Cerebrosphaera* and envelope of *Cerebrosphaera* from the Lancer 1 drill core, Kanpa Formation, depths 680.10 m; C: specimen of *Cerebrosphaera* from the Empress 1A drill core, Kanpa Formation depth 736. 33 m; D: specimen of *Cerebrosphaera* from the Svanbergfjellet Formation and E: freshly hatched egg of *Artemia*. Temperatures estimated with Raman microspectroscopy are indicated at the upper right corner of each spectrum of the fossil material.All specimens of *Cerebrosphaera* and their envelope show similar band distribution, evidencing an aromatic biopolymer composition, with aliphatic and ether bonds. Spectra obtained on specimens from the Svanbergfjellet Formation show the presence of more aromatic bands due to their higher thermal maturity, which enhanced the aromaticity. Fresh *Artemia*'s eggs show a different spectrum similar to a representative α-chitin spectrum as show on Table 5, and characterized by the absence of aromatic bonds and presence of amide bonds. The insert shows representative specimens.

Table 5
FTIR spectra band assignments for *Cerebrosphaera, Artemia* and alpha-chitin standard. Band assignments follow Larkin (2011) for the specimens of *Cerebrosphaera* and *Artemia,* and Ehrlich et al. (2013) for the alpha chitin standard. O. ph: out of phase; i. ph: in phase; str.: stretching; ben.: bending

Cerebrosphaera (Lancer 1. Australia)		*Cerebrosphaera* (Empress 1A Australia)		*Cerebrosphaera* (Spitsberg)		Artemia egg		Alpha-chitin standard Ehrlich et al. (2013)	
positon	liaison	position	liaison	position	liaison	position	liaison	position	liaison
				3640	O–H str. (free radical)	3594.4	O–H str. (free radical)		
3445–3400	O–H str.	3445–3400	O–H str.	3445–3400	O–H str.				
3400		3400		3400					
						3288.3	NH str. (O = C-NH-)	3265	NH str.
3222–3200		3222–3200		3222–3200					
						3100	Overtone CNH stretch/bend (O = C-NH-)		
3055–3045	aryl CH str.	3055–3045	aryl CH str.	3055–3045	aryl CH str.				
2975–2950	Methyl R-CH_3 o. ph. str.	2975–2950	Methyl R-CH_3 o. ph. str.	2975–2950	Methyl R-CH_3 o. ph. str.	2959.5	CH_3 o. ph. Stretching (R-CH_3)	2965	CH3 stretching
2925–2920	Methylene R-CH_2 o. ph. str.	2925–2920	Methylene R-CH_2 o. ph. str.	2925–2920	Methylene R-CH_2 o. ph. str.	2923.9	CH_2 o. ph. Stretching (R-CH_2-R)	2932	C–H stretching (chitin). (γ (COCH3))
3000–2880	CH stretching (O = C–H)	3000–2880	CH stretching (O = C–H)	3000–2880	CH stretching (O = C–H)	2896.7	CH stretching (O = C–H)		
								2877	CH2 stretching (pyranose ring)/C–H stretching
2865–2860	Methylene R-CH_2 i. ph. str.	2865–2860	Methylene R-CH_2 i. ph. str.	2865–2860	Methylene R-CH_2 i. ph. str.				
2860–2855	Methyl R-CH_3 i. ph. str.	2860–2855	Methyl R-CH_3 i. ph. str.	2860–2855	Methyl R-CH_3 i. ph. str.	2852.5	CH_3 i. ph. Stretching (R-CH_3)		
				1910	Cumulated Diene > C = C = C o. ph. str.				
						1743.4	C = O stretching (R-CO-H)		
						1646	NH_2 bend (O = C-NH_2)	1658	Amide I band
1610–1595	Aromatic ring quadrant str.	1610–1595	Aromatic ring quadrant str.	1610–1595	Aromatic ring quadrant str.				
						1536.8	CNH stretch/bend (O = C-NH-)	1556	Amide II band
1513–1509	Aromatic ring semicircles str.	1513–1509	Aromatic ring semicircles str.	1513–1509	Aromatic ring semicircles str.				
						1460.1	CH_2 bend (R-CH_2-R)	1464	CH2 bending (pyranose ring)
1450–1420	Methylene O = C-CH_2 ben.	1450–1420	Methylene O = C-CH_2 ben.	1450–1420	Methylene O = C-CH_2 ben.	1430.6	CH_2 bend (O = C-CH_2)		
1390–1365	Methyl O = C-CH_3 i. ph. ben.	1390–1365	Methyl O = C-CH_3 i. ph. ben.	1390–1365	Methyl O = C-CH_3 i. ph. ben.				
1360–1320	R3CH CH ben.								
1250–1230	Ether Ar-O-CH_2 str.	1250–1230	Ether Ar-O-CH_2 str.	1250–1230	Ether Ar-O-CH_2 str.	1250–1230	Ether Ar-O-CH_2 str.		
1155–1125	Ether R-C-OH str.	1155–1125	Ether R-C-OH str.	1155–1125	Ether R-C-OH str.			1156	C-O stretching
1090–1070	Ether R-C-OH str.	1090–1070	Ether R-C-OH str.	1090–1070	Ether R-C-OH str.				
						1107.8	CH_2-O-CH_2 COC o. ph. str.		
								1072	C-O stretching
1040–1030	Methylene AR-O-CH_2 def.	1040–1030	Methylene AR-O-CH_2 def.	1040–1030	Methylene AR-O-CH_2 def.				
				875–870	Various aromatic rings vibrations				
				850–830					
				830–800					
				755–745					
		730–720	Various aromatic rings vibrations	730–720					
						711.5	$(CH_2)_{>3}$ i.ph. twist		
				675–620	Aromatic ring i. pla. ben.				

Table 6
Comparison between *Cerebrosphaera* and potential analogues.

	Cerebrosphaera (acritarch) (this study)	*Megasphaera ornata* (microfossil)	*Gyalsosphaeridium sp.* (acritarch)	Crustaceans eggs	Sponges eggs	Cnidaria eggs	Placozoan eggs	Prasinophyte Phycomata	Algae	Dynocysts
Diameter	55–650 µm	200–850 µm (Zhang and Zhang, 2017)	112–371 µm (Grey, 2005)	Vary according to species. From 105.3 to 127 in McLaren (1965) for copepods; from 270 to 380 in Belk (1977) for shrimps; from 0.03 mm^3 to 0.09 mm^3 for amphipods (Shaeder 1996)	100–120 µm (Boury-Esnault et al., 1999)	120 to 1200 µm (Anthozoans) (Strathmann 1992; Mills and Strathman, 1992); 100 to 300 µm (Hydrozoans) (Mills and Strathman, 1992)	70–120 µm (Eitel et al., 2011)	30–500 µm (Cohen et al., 2009)	Highly variable. from 0.95 µm to 1 mm (Beardall et al., 2009)	20–160 µm (Cohen et al., 2009)
Morphology	Cerebrate morphology	Smooth inner vesicle (Xiao and Knoll, 2000)	With processes (Grey, 2005)	Variable according to species, some showing cerebrate morphology in copepods (Van Waveren, 1993; Samchyshyna and Santer, 2010 (Fig. 1B); Berasategui et al., 2012); lobsters (Martin et al., 2003; Martin et al., 2005); branchiopodes (Belk, 1998 (Fig. 3&4); Mura, 2001 (Plate VI, specimen 7–8); Yan-bin and Di-ying, 2008 (Fig. 3 D-F))	Variable according to species, no cerebrate morphology reported, (Riesgo and Maldonado, 2009)	Variable according to species, no cerebrates morphologies reported (Honneger, 1983; Piraino, 1992)	Eggs constantly encompassed in the individuals (Eitel et al., 2011)	Smooth exterior	Variable according to species, no cerebrates morphologies	polygonal (paratabulation) with processes in some. No cerebrate morphologies
	presence of a smooth envelope around the cerebrate vesicle	Envelope with complex morphologies, one being cerebrate (Xiao and Knoll, 2000)	No envelope (Grey, 2005)	Smooth envelope encapsulating one egg	Smooth envelope encapsulating several cells (Riesgo and Maldonado, 2009)	no envelope	No envelope (Eitel et al., 2011)	No envelope	Variable within species	No envelope
Complex ultrastructure	Presence of two or three different layers	unknown	Multilayered wall (Cohen et al., 2009, Willman, 2009)	Variable according to species, often complex in diapause eggs (Santella and Ianora, 1990; Ianora and Santella, 1991; Couch et al., 2001; Samchyshyna and Santer, 2010; Berasategui et al., 2012)	Multiple very thin layers (Riesgo and Maldonado, 2009))	Thin membrane, sometimes a protective coating (Honneger, 1983; Piraino, 1992)	Thin membrane (Eitel et al., 2011)	One thick layer marked by radial canals and pores (Moestrup et al., 2003)	Ranging from one layer to several layers	Multilayered wall (Kokinos, 1994)
Excystment or egg opening structure	Either irregular tiering, or no opening but variable state of preservation	No opening reported in species description (Xiao and Knoll, 2000)	No opening reported in species description (Grey, 2005)	Irregular or partial splits in *Artemia* (this study) or by enzymatic weakening of the wall or mechanical movements depending on the species (De Vries and Forward, 1991)	Fecundation inside the sponge and releasing later in the forms of larvae (Osinga et al., 1999)	No opening, transformation of the eggs into embryos and then into planula (Mills and Stratham, 1992)	No opening, transformation of the eggs in embryos and then decay of the adult individual to release floating embryos	Medial rupture along a line of weaknesses (Colbath and Grenfell, 1995)	Variable within the species	Through an archeopyle

(*continued on next page*)

Table 6 (*continued*)

	Cerebrosphaera (acritarch) (this study)	*Megasphaera ornata* (microfossil)	*Gyalosphaeridium sp.* (acritarch)	Crustaceans eggs	Sponges eggs	Cnidaria eggs	Placozoan eggs	Prasinophyte Phycomata	Algae	Dynocysts
Chemistry	aromatic biopolymer	unknown	unknown	Chitin, chitosan and others	Collagen and proteins	Chitin, chitosan and others	unknown	Algaenan, cellulose and other	Algaenan, cellulose and other	Dinosporin, cellulose, and other (Kokinos et al., 1998)
Inferred or known affinity	Stem metazoan egg	Stem metazoan egg (Xiao and Knoll, 2000)	Stem metazoan egg (Cohen et al., 2009)	Metazoan egg	Metazoan egg	Metazoan egg	Metazoan egg	Algal cyst	Algal cyst	Dinoflagellate cyst

conditions (Fell, 1974; Simpson, 1984; Ilan et al., 1996). They have a complex morphology, with, in the case of the genus *Eunapius,* a polygonal gemmular capsule, covering a cluster of spheroidal gemmules with a thick alveolar pneumatic layer and a second collagen layer. These gemmules also show an open micropyle (Ilan et al., 1996). In cnidarians (corals and anemones), the methods of reproduction vary between asexual reproduction and sexual reproduction (Fautin, 2002). The wall ultrastructure of Anthozoans eggs show in general a thin membrane (Honneger, 1983; Piraino, 1992). In some cases, a protective coating can be found, as for *Hydra carnea*, consisting of two different layers, one outer layer 25–40 μm-thick composed of densely packed fibres and an inner layer 3.5 to 6 μm-thick composed of loosely packed fibres (Honneger, 1983). The eggs of the placozoans are simple and generally contained in the adult individual until release when the embryos are already well developed (Eitel et al., 2011).

Comparison between modern copepods eggs and acritarchs has already been suggested by Van Waveren (1993). Willman (2009) compared the ultrastructure of the Ediacaran acritarchs *Gyalosphaeridium pulchrum* to that of the diapause eggs of the copepod *Pontella mediterranea*. The similarities between the two wall ultrastructures, in terms of position and relative thickness of the different layers, combined with the morphological resemblance of *G. pulchrum* with an embryo containing microfossil called *Tianzhushania* (Yin et al., 2008) lead the author to conclude that at least some acritarchs may represent eggs of metazoans (Willman, 2009). Another study reported similarities between the multilayered wall ultrastructure of the shrimp *Brachinella longirostris*'s eggs and the Ediacaran acritarch *Gyalosphaeridium* sp., suggesting that large Ediacaran acanthomorph acritarchs represent stem metazoan eggs (Cohen et al., 2009). The present study shows that well-preserved specimens of *Cerebrosphaera* also possess a tri-layered wall. However, as discussed above, multilayered walls are not unique to metazoan eggs but also occur in protist cysts.

5.2.3. Wall chemistry

Another less common approach to determine the biological affinities of microfossils is the analysis of the wall chemistry. Using micro-infrared spectroscopy, the composition of the biopolymer making up the wall of *Cerebrosphaera* is compared to potential morphological analogues and with other highly resistant and known biopolymers. The FTIR spectra obtained on *Cerebrosphaera* seems to reveal a unique composition unrelated to modern biopolymers, based on our current knowledge. It differs greatly compared to the spectra obtained from the currently known modern biopolymers such as algaenan (Kodner et al., 2009), previously reported in the Ediacaran acritarch *Tanarium* (Marshall et al., 2005) and *Multifronsphaeridium pelorium* (Arouri et al., 1999); chitin (Cardenas et al., 2004; Loron et al., 2019b); 505 Ma old demosponge fossil (Ehrlich et al., 2013) and 200 Ma old gastropod eggs (Wysokowki et al., 2014), or cellulose (Pandey, 1999), by its higher aromaticity. Dinosporin (Bogus et al., 2012) is an aromatic compound but also differs from *Cerebrosphaera* biopolymer. Previous studies have also revealed aromatic compounds in other Proterozoic acritarch walls (Marshall et al., 2005). Here, this aromaticity does not result from the thermal maturity of the specimens, as shown by our microspectroscopy analyses, but is primary. The specimens of Cerebrosphaera from Australia and Svalbard underwent different burial history. Yet the FTIR spectra remain relatively similar (Fig. 9), the specimens from the Svanbergfjellet Formation showing only a slightly more aromatic composition than the specimens coming from the Kanpa Formation. The less thermally mature Australian specimens still show a highly aromatic biopolymer despite a low temperature (Fig. 9C). FTIR spectra of *Artemia* and *Cerebrosphaera* also differ (Fig. 9E); *Cerebrosphaera* specimens show a mostly aromatic biopolymer, with only a small proportion of short aliphatic chains (up to 8 or 10 carbons long). At the opposite, almost no aromatic moieties are present in the spectra of *Artemia* eggs, while the presence of amine bonds and other peaks distribution unsurprisingly, corresponds to the spectra of alpha-chitin

standard detailed by Ehrlich et al. (2013). The chitin biopolymer is quite resistant and has been identified in well-preserved fossils (Ehrlich et al., 2013; Wysokowki et al., 2014; Loron et al., 2019b). Pyrolysis experiment conducted on chitin standard showed that it remains recognisable by FTIR analysis until it reaches a temperature of 230 °C (Wanjun et al., 2005). Therefore, chitin could in theory be preserved in the geological contexts studied here, but was not detected in *Cerebrosphaera*.

5.2.4. Possible metazoan affinities

In summary, our analyses show that the cerebroid morphology, the multilayered wall ultrastructure and the large size of *Cerebrosphaera* are consistent with and uniquely found in some metazoan eggs, although the aromatic biopolymer is so far not comparable to known biopolymers. Challenges persist for the interpretation of acritarchs due to the limited knowledge of modern biopolymers and ultrastructure of protists cysts and vegetative walls, and of metazoan eggs, and to the limits of actualism, as the biopolymers synthesized by stem eukaryotes may differ from those of modern clades. The possibility of morphological convergence is common in evolution and cannot be discarded completely, but the similarity of the distinctive cerebroid morphology and its restricted occurrence in a few clades of modern arthropods is striking. Stem metazoan living in shallow-water marine environments or tidal pools may have produce nonchitinous multi-layered eggs, and may have adopted similar cerebroid morphology to resist desiccation, predation, or other stressful conditions, as modern analogues do (Watanabe, 2006; Mertens et al., 2008). Its combination with similar morphometric and ultrastructural characters, the occurrence of younger Neoproterozoic acritarchs interpreted as metazoan eggs, and estimates from molecular clocks, support our hypothesis of a possible stem metazoan affinity for *Cerebrosphaera*. This hypothesis is consistent with molecular phylogenies, placing the appearance of crustaceans in the Ediacaran or Cryogenian (Pisani et al., 2004) while others place the origin of metazoans in the Cryogenian (Blair and Hedges, 2005; Erwin et al., 2011; Dos Reis et al., 2015). Several studies also suggest that low oxygenation concentration in Proterozoic oceans would not hamper the origin of metazoans (Mills et al., 2018), and might even promote innovations (Wood and Erwin, 2018). A recent review by Xiao and Tang (2018) underlines the absence of animal fossil remains during the Tonian period, reassessing the fossils *Protoarenicola*, *Pararenicola*, and *Sinosabellidites* previously interpreted as worm-like animals (Chen, 1988) or algae (Dong et al., 2008). The oldest fossil record of metazoans reported so far includes microfossils interpreted as animal embryos in the Ediacaran Doushantuo Formation (Chen et al., 2000; Xiao, 2002; Dornbos et al., 2005) and the Australian Tanana Formation (Cohen et al., 2009), and molecular fossils (biomarkers) of demosponges in the Cryogenian (Love et al., 2009; Brocks et al., 2017) or of unspecified metazoans associated with the macrofossil *Dickinsonia* in the Ediacaran (Bobrovskiy et al., 2018), but recent fossil discoveries suggest indirectly an earlier origin (Loron et al., 2019b).

5.3. Implications for Neoproterozoic paleogeography and biostratigraphy

Cerebrosphaera is found worldwide in successions ranging from ~792 to ~738 Ma (Riedman and Sadler, 2017), and reported here for the first time in the Congo craton in Africa. Its narrow stratigraphic range and worldwide distribution (see Fig. 1) confirm the value of this taxon as an interesting biostratigraphic index fossil.

Seven of the locations of *Cerebrosphaera* are intracratonic sedimentary basins linked with the supercontinent Rodinia break up: the Officer and Amadeus basins in Australia (Walter et al., 1995), the Chuar Group in the USA (Timmons et al., 2001, Dehler et al., 2001), the Chichkan Formation in Kazakhstan (Sergeev and Schopf, 2010), the Visingsö Formation in Sweden (Vidal 1985) and the Lena-Anabar Basin in Russia (Nagovitsin et al., 2015). These basins show similar characteristic, with sediments deposited in shallow-water environments. The other three occurrences of *Cerebrosphaera* correspond to passive margins: the Svanbergfjellet, Draken and Ryssö formations in Svalbard (Maloof et al., 2006), the Gouhou Formation in China at the margin of the North China Craton (Tang et al., 2015) and the Burra Group in Australia at the margin of the Gawler Craton (Preiss, 2000). In all these locations, the sediments where *Cerebrosphaera* is preserved show similar characteristics, with low sea level or even restricted environment and an important terrigenous input. This high weathering, caused by the break-up of Rodinia, could have participated to maintain a ferruginous middle water column and thus detoxifying the passive margins (Guilbaud et al., 2015), possibly promoting the development and diversification of eukaryotes in these settings. The relation between redox conditions, nutrient availability and eukaryote diversification proposed by Anbar and Knoll (2002) has been documented by detailed coupled redox and microfossil analyses in the older Taoudeni Basin, where the eukaryotic distribution suggests a possible control by the presence of nutrients and oxygen in shallow environments (Beghin et al., 2017; Baludikay et al., in review) although the lack of time resolution of redox proxies and fossil assemblages prevents definitive conclusions. However, such studies are still rare (Porter et al., 2018) and do not preclude the diversification of anaerobe protists in the Proterozoic (Javaux and Knoll, 2017), nor the origin of metazoans in dysoxic environments (Mills et al., 2018). The cosmopolitan distribution of *Cerebrosphaera* also suggests the presence of connections between the contemporaneous marine basins, and the absence of provincialism, even in restricted or intracratonic basins.

The report of the first occurrence of *Cerebrosphaera* in Africa, in the Bz2 Formation, West Congo Supergroup, Mayombé Group, permits to propose three possible hypotheses regarding the age of the formation. In the first hypothesis, *Cerebrosphaera* appeared later in the Congo Craton, between the Sturtian and Marinoan glaciations. The second hypothesis suggests a pre-Sturtian age in the Congo Craton as its worldwide distribution elsewhere shows. However, *Cerebrosphaera* specimens are preserved here in shales fragments that are reworked and preserved within the black argillite sediments of the younger Cryogenian Bouenza Subgroup. This type of occurrence was previously reported in a study by Riedman et al. (2014), where fragments of *Cerebrosphaera* occurred in the glacial units of the Australian Amadeus Basin and interpreted as reworked materials of the robust walls. In the present study, the fossiliferous shale fragments are reworked, not the fossils themselves directly. In a third hypothesis, *Cerebrosphaera* would be pre-Sturtian and thus the Bouenza Subgroup also.

The available geochronological constraints of the upper diamictite and the Mayombe Group suggest an age younger than 694 Ma and probably older than 635 Ma for the Bouenza/Louila Subgroup (Affaton et al., 2015). These dates tend to infirm the third hypothesis, as it would imply a complete revision of the whole stratigraphy of the region. The second hypothesis seems to be the simpler explanation, supported by the rock facies (unconsolidated mudstone) in which the shale fragments hosting *Cerebrosphaera* are found and previously reported cases of reworking. The first hypothesis remains a possibility but better geochronological constraints are needed to confirm it, and it would be the first and the only occurrence of younger *Cerebrosphaera*.

6. Conclusions

The combination of morphological, ultrastructural and molecular characterization of several specimens of *Cerebrosphaera* supports the recently revised taxonomy, and permits the proposition of a new hypothesis regarding its biological affinities. This microfossil shows a complex and distinctive cerebroid morphology of the vesicle surrounded by a thin envelope, no excystment structure, a multi-layered wall ultrastructure and resilient chemistry, associated with a large diameter range, confirming its classification within the Eukaryota domain. Based on comparison with modern analogues, the hypothesis of a stem metazoan affinity is proposed, consistent with the new data

presented here and with molecular phylogenies, although the biopolymer composition remains unique so far. *Cerebrosphaera* may thus possibly represent the first animal fossil found during the Tonian period. We also report its occurrence in Africa for the first time, confirming the value of *Cerebrosphaera* as an index taxon. Further work is needed on modern eukaryotic eggs or cysts for a finer classification of this important index fossil. Nonetheless it is clear that *Cerebrosphaera* was part of the Neoproterozoic eukaryotic diversification, with other microfossils assigned to eukaryotic crown groups.

Acknowledgments

Research funding came from the European Research Council Stg ELITE FP7/308074, BELSPO IAP PLANET TOPERS, the FRS-FNRS CDR J.0014.18, and the FRS-FNRS-FWO Excellence of Science project ET-HOME grant 30442502. We thank N. Butterfield (University of Cambridge, UK) for providing specimens of *Cerebrosphaera* from the Svanbergfjellet Formation, Spitsbergen; K Grey (GSWA) for access to drill cores in GSWA, Perth, Australia; Y Callec and the BRGM for providing the Bouenza Formation samples; J.-Y. Storme for help with Raman analyses, M. Giraldo (ULiège) for sample preparation, Sarah Smeets (ULiège) for the preparation of ultrathin sections, Stephan Borensztajn (IPG-Paris) for the SEM imagery, S. Porter for comments on a previous draft, and two anonymous reviewers for constructive comments on the present manuscript.

Appendix A. Supplementary data

Supplementary data to this article can be found online at https://doi.org/10.1016/j.precamres.2019.105410.

References

Affaton, P., Kalsbeek, F., Boudzoumou, F., Trompette, R., Thrane, K., Frei, R., 2015. The Pan-African west Congo belt in the Republic of Congo (CongiBrazzaville): stratigraphy of the Mayombe and west Congo Supergroups studied by detrital zircon geochronology. Precambr. Res. 272, 185–202.

Agić, H., Moczydłowska, M., Yin, L.M., 2015. Affinity, life cycle, and intracellular complexity of organic-walled microfossils from the Mesoproterozoic of Shanxi, China. J. Paleontol. 89 (1), 28–50.

Al-Ameri, T., Wicander, R., 2008. An assessment of the gas generation potential of the Ordovician Khabour Formation, Western Iraq. Comunicações Geológicas 95, 157–166.

Anbar, A.D., Knoll, A.H., 2002. Proterozoic ocean chemistry and evolution: a bioinorganic bridge? Science 297 (5584), 1137–1142.

Anderson, E., Lochhead, J.H., Lochhead, M.S., Huebner, E., 1970. The origin and structure of the tertiary envelope in thick-shelled eggs of the brine shrimp, Artemia. J. Ultra. Res. 32 (5–6), 497–525.

Antcliffe, J.B., 2013. Questioning the evidence of organic compounds called Sponge Biomarkers. Paleontology 56 (5), 917–925. https://doi.org/10.1111/pala.12030.

Archibald, D., Glorie, S., Muanza-Kant, P., Baudet, D., Kanda-Nkula, V., Kitambla-Yaya, N., Mpiana-Kenababo, C., Nseka-Mbemba, P., Tack, L., 2018. The lower diamictite formation of the Cataractes Group, West Congo supergroup (Bas-Congo region, DR Congo): a 678 My marker of extensional episodic activity during breakup of Columbia. CAG 27 Aveiros abstracts, p19.

Arouri, K.R., Greenwood, P.F., Walter, M.R., 1999. A possible chlorophycean affinity of some Neoproterozoic acritarchs. Org Geochem. 30, 1323–1337.

Arouri, K.R., Greenwood, P.F., Walter, M.R., 2002. Biological affinities of Neoproterozoic acritarchs from Australia: microscopic and chemical characterization. Org Geochem. 31, 75–89.

Atkinson, A.W., Gunning, B.E.S., John, P.C.L., 1972. Sporopollenin in the cell wall of Chlorella and other algae: ultrastructures, chemistry, chemistry and incorportation of 14C-acetate, studied in synchronous culture. Planta 107, 1–32.

Baludikay, B.K., François, C., Sforna, M.C., Beghin, J., Cornet, Y., Storme, J.-Y., Fagel, N., Fontaine, F., Littke, R., Baudet, D., Delvaux, D., Javaux, E.J., 2018. Raman microspectroscopy, bitumen reflectance and illite crystallinity scale: comparison of different geothermometry methods of fossiliferous Proterozoic sedimentary basins (DR Congo, Mauritania and Australia). Int. J. Coal Geol. 191, 80–94.

Barker, C.E., Pawlewicz, M.J., 1994. Calculation of Vitrinite Reflectance from thermal Histories and Peak Temperatures. A Comparison of Methods. ACS Sysmposium series 570, 216–229.

Beardall, J., Allen, D., Bragg, J., Finkel, Z.V., Flynn, K.J., Quigg, A., Rees, T.A.V., Richardson, A., Raven, J.A., 2009. Allometry and stoichiometry of unicellular, colonial and multicellular phytoplankton. New Phytol. 181 (2), 295–309.

Beghin, J., Guilbaud, R., Poulton, S.W., Gueneli, N., Brocks, J.J., Storme, J.-Y., Blanpied, C., Javaux, E.J., 2017. A palaeoecological model for the late Mesoproterozoic – early Neoproterozoic Atar/El Mreïti Group, Taoudeni Basin, Mauritania, northwestern Africa. Precambr. Res. 299, 1–14.

Belk, D., 1977. Evolution of the egg size strategies in fairy shrimps. The Southwestern Naturalist 22 (1), 99–105.

Belk, D., Mura, G., Weeks, S.C., 1998. Untangling confusion between *Eubranchipus vernalis and Eubranchypus neglectus* (Branchiopoda: Anostraca). J. Crustac. Biol. 18 (1), 147–152.

Bengtson, S., Sallstedt, T., Belivanova, V., Whitehouse, M., 2017. Three-dimensional preservation of cellular and subcellular structures suggests 1.6 billion-year-old crown-group red algae. PLoS Biol. 15 (3), 38p. https://doi.org/10.1371/journal.pbio.2000735.

Berasategui, A.A., Hoffmeyer, M.S., Dutto, M.S., Biancalana, F., 2012. Seasonal variation in the egg morphology of the copepod Eurytemora americana and its relationship with reproductive strategy in a temperate estuary in Argentina. ICES J. Mar. Sci. 69 (3), 380–388. https://doi.org/10.1093/icesjms/fsr192.

Blair, J.E., Hedges, S.B., 2005. Molecular Phylogeny and Divergence Times of Deuterostome Animals. Mol. Biol. Evol. 22 (11), 2275–2284.

Bobrovskiy, I., Hope, J.M., Ivanstov, A., Nettersheimn, B.J., Hallmann, C., Brocks, J.J., 2018. Ancient steroids establish the Ediacaran fossil *Dockinsonia* as one of the earliest animals. Science 361, 1246–1249.

Bogus, K., Harding, I.C., King, A., Charles, A.J., Zonneveld, K.A.F., Versteegh, G.J.M., 2012. The composition and diversity of the *Apectodinium* complex (Dinoflagellata). Rev. Palaeobot. Palynol. 183, 21–31.

Bosak, T., Lahr, D.J., Gooday, A.J., Dalton, L., Matys, E.D., 2012. Possible early foraminiferans in post-Sturtian (716–635 Ma) cap carbonates. Geology 40 (1), 67–70. https://doi.org/10.1130/G32535.1.

Boury-Esnault, N., Efremova, S., Bezac, C., Vacelet, J., 1999. Reproduction of a hexactinellid sponge: first description of gastrulation by cellular delamination in the Porifera. Invertebrate Reproduction and Development 35 (3), 187–201.

Brocks, J.J., Jarrett, A.J.M., Sirantoine, E., Hallmann, C., Hoshino, Y., Lyanage, T., 2017. The rise of algae in Cryogenian oceans and the emergence of animals. Nature 548, 578–581.

Butterfield, N.J., 2001. Bangiomorpha pubescens n. gen., n. sp.: implications for the evolution of sex, multicellularity, and the Mesoproterozoic/ Neoproterozoic radiation of eukaryotes. Paleobiology 26 (3), 386-404.

Butterfield, N.J., 2004. A Vaucherian alga from the middle Neoproterozoic of Spitsbergen: implications for the evolution of Proterozoic eukaryotes and the Cambrian explosion. Paleobiology 30 (2), 231–251.

Butterfield, N.J., Knoll, A.H., Sweet, K., 1994. Paleobiology of the Neoproterozoic Svanbergfjellet Formation, Spitsbergen. Fossils Strata 34, 82.

Cabeen, M.T., Jacobs-Wagner, C., 2007. Skin and bones: the bacterial cytoskeleton, cell wall, and cell morphogenesis. J. Cell Biol. 179 (3), 381–387.

Cahen, L., 1978. La stratigraphie et la tectonique du Supergroupe Ouest-Congolien dans les zones médiane et externe de l"orogenèse Ouest-Congolien (Pan-Africain) au Bas-Zaïre et dans les régions voisines. Annales du Musée Royal de l"Afrique Centrale, Tervuren, in 8°. Sciences Géologiques 83, 150.

Calver, C.R., Black, L.P., Everad, J.L., Seymour, D.B., 2004. U-Pb zircon age constraints on late Neoproterozoic glaciation in Tasmania. Geology 32 (10), 893–896. https://doi.org/10.1130/G20713.1.

Cardenas, G., Cabrera, G., Taboada, E., Miranda, S.P., 2004. Chitin characterization by SEM, FTIR, XRD, and 13C cross polarization/mass angle spinning NMR. J. Appl. Polym. Sci. 93, 1876–1885.

Cavalier-Smith, T., 2002. The Neomuran Origin of Archaebacteria, the Negibacteria Root of the Universal Tree and Bacteria Megaclassification. Int. J. Syst. Microbiol. 52, 7–76.

Charles, N., Callec, Y., Préat, A., Thiéblemont, D., Delpomdor, F., Malounguila, D., Gloaguen, E., Petitot, J., Akouala, A.-P., Ndiele, B., Mvoula Boungou, I., Moebo Boungou, M., 2015. Notice explicative de la carte géologique de la République du Congo à 1/200 000. Feuille Madingou, Editions BRGM.

Chen, J., 1988. Precambrian metazoans of the Huai River drainage area (Anhui, E. China): their taphonomic and ecological evidence. Senckenb. Lethaea 69, 189–215.

Chen, J.Y., Oliveri, P., Li, C.-W., Zhou, G.-Q., Gao, F., Hagardorn, J.W., Peterson, K.J., Davidson, E.H., 2000. Precambrian animal diversity: putative phosphatized embryos from the Doushantuo Formation of China. PNAS 97 (9), 4457–4462.

Coates, J., 2000. 2000. Interpretation of infrared Spectra, a practical approach. In: Meyers, R.A. (Ed.), Encyclopedia of Analytical Chemistry. John Wiley & Sons Ltd, Chichester.

Cohen, P.A., Macdonal, F.A., 2015. The Proterozoic record of Eukaryotes. Paleobiology 41 (4), 610–632.

Cohen, P.A. Riedman, L.A., 2018. It's a protist-eat-protist world: recalcitrance, predation, and evolution in the Tonian–Cryogenian ocean. Emerging Topics in Life Sciences, ETLS20170145. https://doi.org/10.1042/ETLS20170165.

Cohen, P.A., Knoll, A.H., Kodner, R.B., 2009. Large spinose microfossils in Ediacaran rocks as resting stages of early animals. PNAS 106 (16), 6519–6524.

Cohen, P.A., Strauss, J.V., Rooney, A.D., Sharma, M., Tosca, N., 2017. Controlled hydroxyapatite biomineralization in an ~810 million-year-old unicellular eukaryote. Sci. Adv. 3, e1700095. https://doi.org/10.1126/sciadv.1700095.

Colbath, G.K., 1983. Fossil prasinophycean phycomata from the Silurian Braibridge Formation, Missouri, U.S.A. Phycologia 22(3), 249-255.

Colbath, G.K., Grenfell, H.R., 1995. Review of biological affinities of Paleozoic acid-resistant, organic-walled eukaryotic algal microfossils (including “acritarchs”). Rev. Palaeobot. Palynol. 86, 287–314.

Cotter, K.L., 1999. Microfossils from Neoproterozoic Supersequence 1 of the Officer Basin, Western Australia. Alcheringa 23, 63–86. https://doi.org/10.1080/03115519908619323.

Couch, K.M., Downes, M., Burns, C.W., 2001. Morphological differences between subitaneous and diapause eggs of Boeckella triarticulata (Copepoda: Calanoida). Freshw. Biol. 46, 925–933.
De Vries, M.C., Forward, J.R., 1991. Mechanisms of crustacean egg hatching: evidence for enzyme release by crab embryos. Mar. Biol. 110, 281–291.
Dehler, C.M., Elrick, M.E., Karlstrom, K.E., Smith, G.A., Crossey, L.J., Timmons, M.J., 2001. Neoproterozoic Chuar Group (~800–742 Ma), Grand Canyon: a record of cyclic marine deposition during global climatic and tectonic transition. Sed. Geol. 141–142, 465–499.
De Leeuw, J.W., Versteegh, G.J.M., van Bergen, P.F., 2006. Biomacromolecules of algae and plants and their fossils analogues. Plant Ecol. 182, 209–233.
Delpomdor, F., Kant, F., Préat, A., 2014. Neoproterozoic uppermost Haut-Shiloango Subgroup (West Congo Supergroup, DRC): Misinterpreted stromatolites and implications for sea-level fluctuations before the onset of the Marinoan glaciation. J. Afr. Earth Sc. 90, 49–63.
Emerg. Top. Life Sci. 2 (2), 235–245. https://doi.org/10.1042/ETLS20170146.
Dong, X., 2009. Cambrian fossil embryos from western Hunan, South China. Acta Geologica Sinica 83 (3), 429–439.
Dong, L., Xiao, S., Shen, B., Yuan, X., Yan, X., Peng, Y., 2008. Restudy of the worm-like carbonaceous compression fossils *Protoarenicola*, *Pararenicola*, and *Sinosabellidites* from early Neoproterozoic successions in North China. Palaeogeogr. Palaeoclimatol. Palaeoecol. 258, 138–161.
Dornbos, S.Q., Bottjer, D.J., Chen, J.-Y., Oliveri, P., Gao, F., Li, C.-W., 2005. Precambrian animal life: taphonomy of phophatized metazoan embryos from southwest China. Lethaia 38, 101–109.
Dos Reis, M., Thawornwattana, Y., Angelis, K., Telford, M.J., Donoghue, P.C.J., Yang, Z., 2015. Uncertainty in the timing of Origin of Animals and the Limits of Precision in Molecular Timescales. Curr. Biol. 25, 2939–2950.
Ehrlich, H., Rigby, J.K., Botting, J.P., Tsurkan, M.V., Werner, C., Schwile, P., Petrášek, Z., Pisera, A., Simon, P., Sivkov, V.N., Vyalikh, D.V., Molodtsov, S.L., Kurek, D., Kammer, M., Hunoldt, M., Born, R., Stawski, D., Steinhof, A., Bazhenov, V.V., Geisler, T., 2013. Discovery of 505-million-year old chitin in the basal demosponge *Vauxia gracilenta*. Sci. Rep. 3, 3497.
Eitel, M., Guidi, L., Hadrys, H., Balsamo, M., Schierwater, B., 2011. New insights into Placozoan Reproduction and Development. PLoS ONE 6 (5), e19639.
Ereskowsky, A.V., 2000. Reproduction cycles and strategies of the cold-water sponges *Halisarca dujardini* (Demospongiae, Halisarcida, *Myxilla incrustans*, and *Iophon piceus* (Demospongiae, Poecilosclerida) from the White Sea. Biol. Bull. 198, 77–87.
Erwin, D.H., Laflamme, M., Tweedt, S.M., Sperling, E.A., Pisani, D., Peterson, K.J., 2011. The Cambrian Conundrum: early divergence and later ecological success in the early history of animals. Science 334, 1091–1097.
Evans, D.A., 2009. The palaeomagnetically viable, long-lived and all-inclusive Rodinia supercontinent reconstruction. Geol. Soc. London, Spec. Public. 327 (1), 371–404.
Evitt, W.R., 1963. A discussion and proposals concerning fossils Dinoflgellates, Hystrichospheres, and Acritarchs, I*. In: Proceedings of the National Academy of Sciences of the United State of America 49 (2), pp. 158–164.
Eyles, N., 2008. Glacio-epochs and the supercontinent cycle after ~3.0 Ga: Tectonic boundary conditions for glaciations. Palaeogeogr. Palaeoclimatol. Palaeoecol. 258 (1–2), 89–129.
Eyles, C.H., Eyles, N., Grey, K., 2007. Palaeoclimate implications from deep drilling of Neoproterozoic strata in the Officer Basin and Adelaide Rift Complex of Australia; a marine record of wet-based glaciers. Palaeogeogr. Palaeoclimatol. Palaeoecol. 248 (3–4), 291–312.
Fanid, L.M., Seidgar, M., Takami, G.A., 2007. A comparative SEM morphological study on the egg shell in some Anostracans (Crustacea: branchiopoda) from East Azerbaijan province of Iran. Iranian J. Fisheries Sci. 7 (1), 101–110.
Fautin, D.G., 2002. Reproduction of Cnidaria. Canadia J. Zool. 80, 1735–1754.
Fanning, C.M., Link, P.K., 2004. U-Pb SHRIMP ages of Neoproterozoic (Sturtian) glaciogenic Pocatello Formation, southeastern Idaho. Geology 32 (10), 881–884. https://doi.org/10.1130/G20609.1.
Fell, P.E., 1974. Diapause in the gemmules of the marine sponge Haliclona loosanofi, with a note on the gemmules of Haliclona oculate. Biol. Bull. 147, 333–351.
Fensome, R.A., Taylor, F.J.R., Norris, G., Sarjeant, W.A.S., Wharton, D.I., Williams, G.L., 1993. A classification of living and fossils dinoflagellates. Micropaleontology Press, Special Publication 7, 1–351.
Fernandez-Alonso, M., Baudet, D., Thielblemont D., Callec, Y., 2018. The Araçuaí (Brasiliano)-West Congo (Pan African) orogenic system: an updated GIS compilation. CAG 27 Aveiros abstracts, p. 33.
Foissner, W., Muller, H., Weisse, T., 2005. The unusual, lepidosome-coated resting cyst of Meseres corlissi (Ciliophora: Oligotrichea): light and scanning electron microscopy, cytochemistry. Acta protozoologica 44 (3), 201.
Frimmel, H.E., Tack, L., Basei, M.S., Nutman, A.P., Boven, A., 2006. Provenance and chemostratigraphy of the Neoproterozoic West Congolian Group in the Democratic Republic of Congo. J. Afr. Earth Sc. 46, 221–239.
Fullgraf, T., Callec, Y., Thiéblemont, D., Gloaguen, E., Charles, N., Le Métour, J., Prian, J.-P., Boudzoumou, F., Delhaye-Prat, V., Moreau, F., Kebi-Tsoumou, S., Ndiele, B., 2015. Notice explicative de la carte géologique de la République du Congo à 1/200 000, Feuille Dolisie. Éditions BRGM.
Gibson, T.M., Shih, P.M., Fischer, W.W., Crockford, P.M., Hodgskiss, M.S.W., Wörndle, S., Creaser, R.A., Rainbird, R.H., Skulski, T.M., Halverson, G.P., 2018. Precise age of Bangiomorpha pubescens dates the origin of eukaryotic photosynthesis. Geology 46 (2), 135–138. https://doi.org/10.1130/G39829.1.
Graham, L.E., Wilcox, L.W., 2000. Algae: Upper Saddle River NJ. Prentice Hall, pp. 640.
Graham, L.E., Cook, M.E., Wilcox, L.W., Grahal, J., Taylor, W., Wellman, C.H., Lewis, L., 2013. Resistance of filamentous chlorophyceaen, ulvophycean, and xanthophycean algae to acetolysis: testing Proterozoic and Paleozoic microfossil attributions. Int. J. Plants Sci. 174 (6), 947–957.
Graham, L.E., Trest, M.T., Cook, M.E., 2017. Acetolysis Resistance of Modern Fungi: Testing Attributions of Enigmatic Proterozoic and Early Paleozoic Fossils. Int. J. Plant Sci. 178 (4), 330–339.
Grey, K., 1999. Modified palynological preparation technique for the extraction of large Neoproterozoic acanthomorph acritarchs and other acid insoluble microfossils. Geological Survey of Western Australia, Record 1990/10 23.
Grey, K., 2005. Ediacaran palynology of Australia. Memoire of the Association of Australasian Palaeontologists 31, 1–439.
Grey, K., Hill. A.C., Calver C., 2011. Biostratigraphy and stratigraphic subdivision of Cryogenian successions of Australia in a global context. In: Arnaud, E., Halverson, G. P., Shields-Zhou, G., eds, The Geological Record of Neoproterozoic Glaciations, Geological Society, London, Memoirs, 36, 113-134.
Guilbaud, R., Poulton, S.W., Butterfield, N.J., Zhu, M., Shields-Zhou, G.A., 2015. A global transition to ferruginous conditions in the early Neoproterozoic oceans. Nat. Geosci. 8, 466–470.
Hagen, C., Siegmund, S., Braune, W., 2002. Ultrastructural and chemical changes in the cell wall of *Haematococcus pluvialis* (Volvocales, Chlorophyta) during aplanospore formation. Eur. J. Phycol. 37, 217–226. https://doi.org/10.1017/S0967026202003669.
Halverson, G.P., Hoffman, P.F., Schrag, D.P., Maloof, A.C., Rice, A.H.N., 2005. Toward a Neoproterozoic composite carbon-isotope record. GSA Bulletin 117 (9), 1181–1207.
Halverson, G.P., Maloof, C.A., Schrag, D.P., Dudás, F.Ö., Hurtgen, M., 2007. Stratigraphy and geochemistry of a ca 800 Ma negative carbon isotope interval in northeastern Svalbard. Chem. Geol. 237, 5–27. https://doi.org/10.1016/j.chemgeo.2006.06.013.
Hammarlund, E.U., 2018. Valuable snapshots of deep time. Nat. Geosci. 11, 298–299.
Head, M.J., 1996. Chapter 30. Modern Dinoflagellate cysts and their biological affinities. Palynology; principles and applications Vol. 3, 1197–1248.
Hill, A.C., Cotter, K.L., Grey, K., 2000. Mid-Neoproterozoic biostratigraphy and isotope stratigraphy in Australia. Precambr. Res. 100, 281–298.
Hill, A.C., Haines, P.W., Grey, K., 2011. Chapter 67 Neoproterozoic glacial deposits of central Australia. In: Arnaud, E., Halverson, G.P., Shields-Zhou, G. (eds) The Geological Record of Neoproterozoic Glaciations, Geological Society, London, Memoirs 36, 677–691.
Honneger, T.G., 1983. Ultrastructural and experimental investigations of Sperm-Eggs interactions in fertilization of *Hydra carnea*. Roux's Arch. Dev. Biol. 192, 13–20.
Huntley, J., Xiao, S., Kowalewski, M., 2006. 1.3 Billion years of acritarch history: An empirical morphospace approach. Precambr. Res. 144 (1–2), 52–68. https://doi.org/10.1016/j.precamres.2005.11.003.
Ianora, A., Santella, L., 1991. Diapause embryos in the neustonic copepod *Anomalocera patersoni*. Mar. Biol. 108, 387–394.
Igisu, M., Ueno, Y., Shimojima, M., Nakashima, S., Awramik, S.M., Ohta, H., Maruyama, S., 2009. Micro-FTIR spectroscopic signatures of Bacterial lipids in Proterozoic microfossils. Precambr. Res. 173, 19–26. https://doi.org/10.1016/j.precamres.2009.03.006.
Ilan, M., Dembo, M.G., Gasith, A., 1996. Gemmules of sponges from a warm lake. Freshw. Biol. 35, 165–172.
Javaux, E.J., Marshal, C.P., 2006. A new approach in deciphering early protest paleobiology and evolution: combined microscopy and microchemistry of single Proterozoic acritarchs. Rev. Palaeobot. Palynol. 139, 1–15. https://doi.org/10.1016/j.revpalbo.2006.01.005.
Javaux, E.J., 2011. Early eukaryotes in Precambrian oceans. In: Origins and evolution of life. An astrobiological perspective 6. pp. 414.
Javaux, E.J., Knoll, A.H., 2017. Micropaleontology of the lower Mesoproterozoic Roper Group, Australia, and implications for early eukaryotic evolutions. J. Paleontol. 91 (2), 199–229.
Javaux, E.J., Knoll, A.H., Walter, M.R., 2001. Morphological and ecological complexity in early eukaryotic ecosystems. Nature 412, 66–69.
Javaux, E.J., Knoll, A.H., Walter, M.R., 2003. Recognizing and interpreting the fossils of early eukaryotes. Orig. Life Evol. Biosph. 33, 75–94.
Javaux, E.J., Knoll, A.H., Walter, M.R., 2004. TEM evidences for eukaryotic diversity in mid-Proterozoic oceans. Geobiology 2, 121–132.
Javaux, E.J., Marshall, C.P., Bekker, A., 2010. Organic-walled microfossils in 3.2-billion-year-old shallow-marine siliciclastic deposits. Nature 463, 934–938. https://doi.org/10.1038/nature08793.
Jux, U., 1969. Ueber den Feinbau der Zystenwandung von *Pachysphaera marshalliae* Parke 1966. Palaeontographica Abt B 125, 104–110.
Knoll, A.H., Swett, K., Mark, J., 1991. Paleobiology of a Neoproterozoic tidal flat/lagoonal complex: the Draken Conglomerate Formation, Spitsbergen. J. Paleontol. 65, 531–570.
Knoll, A.H., Calder, S., 1983. Microbiotas of the late Precambrian Ryssö Formation, Nordaustlandet, Svalbard. Palaeontology 26 (3), 467–496.
Knoll, A.H., Javaux, E.J., Hewitt, D., Cohen, P., 2006. Eukaryotic organisms in Proterozoic oceans. Philos. Trans. R. Soc. Lond. Ser. B, Biol. Sci. 361 (1470), 1023–1038. https://doi.org/10.1098/rstb.2006.1843.
Kodner, R.B., Pearson, A., Summons, R.E., Knoll, A.H., 2008. Sterols in red and green algae: quantification, phylogeny, and relevance for the interpretation of geologic steranes. Geobiology 6, 411–420.
Kodner, R.B., Summons, R.E., Knoll, A.H., 2009. Phylogenic investigations of the aliphatic, non-hydrolizable biopolymer algaenan, with a focus on green algae. Org Geochem. 40, 854–862.
Kokinos, J.P., 1994. Studies on the cell wall of dinoflagellate resting cysts: Morphological development, ultrastructure, and chemical composition. Ph.D. Thesis, Massachusetts Institute of Technology/Woods Hole Oceanographic Institution, Technical Report WHOI-94-10 234.
Kokinos, J.P., Eglinton, T.I., Gonä, M.A., Boon, J.J., Martoglio, P.A., Anderson, D.M.,

1998. Characterization of a highly resistant biomacromolecular material in the cell wall of marine dinoflagellate resting cyst. Org Geochem. 28 (5), 265–288.
Lahfid, A., Beyssac, O., Deville, E., Negro, F., Chopin, C., Goffé, B., 2010. Evolution of the Raman spectrum of carbonaceous material in low-grade metasediments of the Glarus Alps (Switzerland). Terra Nova 22, 354–360. https://doi.org/10.1111/j.1365- 3121.2010.00956.x.
Larkin, P., 2011. Infrared and Raman spectroscopy principles and spectral interpretation. Elsevier, USA, pp. 230.
Lonsdale, D.J., Levinton, J.S., 1985. Latitudinal differentiation in embryonic duration, egg size, and newborn survival in a Harpacitoid copepod. Biol. Bull. 168, 419–431.
Loron, C.C., François, C., Rainbird, R.H., Turner, E.C., Borensztajn, S., Javaux, E.J., 2019b. Early fungi from the proterozoic era in Arctic Canada. Nature 570, 232–235.
Loron, C.C., Rainbird, R.H., Turner, E.C., Greenman, J.W., Javaux, E.J., 2019a. Organic-walled microfossils from the late Mesoproterozoic to early Neoproterozoic lower Shaler Supergroup (Artic Canada): Diversity and biostratigraphic significance. Precambr. Res. 321, 349–374.
Li, Z.X., Bogdanova, S.V., Collins, A.S., Davidson, A., De Waele, B., Ernst, R.E., Fitzsimons, I.C.W., Fuck, R.A., Glakpchub, D.P., Jacobs, D.P., Karlstrom, K.E., Lu, S., Natapov, L.M., Pease, V., Pisarevsky, S.A., Thrane, K., Vernikovsky, V., 2008. Assembly, configuration, and break-up history of Rodinia: a synthesis. Precambr. Res. 160 (1–2), 179–210. https://doi.org/10.1016/j.precamres.2007.04.021.
Li, Z.X., Evans, D.A., Halverson, G.P., 2013. Neoproterozoic glaciations in a revised global palaeogeography from the breakup of Rodinia to the assembly of Gondwanaland. Sediment. Geol. 294, 219–232.
Lin, R., Ritz, G.P., 1993. Studying individual macerals using i.r. microspectroscopy, and implications on oil versus gas/condensate proneness and low rank generation. Org Geochem. 20, 695–706.
Liu, D.H., Xiao, X.M., Tian, H., Min, Y.S., Zhou, Q., Cheng, P., Shen, J.G., 2013. Sample maturation calculated using Raman spectroscopic parameters for solid organics: methodology and geological applications. Chin. Sci. Bull. 58, 1258–1298.
Love, G.D., Summons, R.E., 2015. The Molecular record of Cryogenian sponges – a response to Antcliffe (2013). Palaeontology 58 (6), 1131–1136.
Love, G.D., Grosjean, E., Stalvies, C., Fike, D.A., Grotzinger, J.P., Bradley, S.A., Kelly, A.E., Bhatia, M., Meredith, W., Snape, C.E., Bowring, S.A., Condon, D.J., Summons, R.E., 2009. Fossils steroids record the appearance of Demospongiae during the Cryogenian period. Nature 457, 718–722.
Lyons, T.W., Reinhard, C.T., Planavsky, N.J., 2014. The rise of oxygen in Earth's early ocean and atmosphere. Nature 506, 307–315. https://doi.org/10.1038/nature13068.
Macdonald, F.A., Schmitz, M.D., Crowley, J.L., Roots, C.F., Jones, D.S., Maloof, A.C., Strauss, J.V., Phoebe, A.C., David, T.J., Schrag, D.P., 2010. Calibrating the Cryogenian. Science 327 (5970), 1241–1243. https://doi.org/10.1126/science.1183325.
Maloof, A.C., Halverson, G.P., Kirschvink, J.L., Schrag, D.P., Weiss, B.P., Hoffman, P.F., 2006. Combined paleomagnetic, isotopic, and stratigraphic evidence for true polar wander from the Neoproterozoic Akademikerbreen Group, Svalbard, Norway. GSA Bull. 118 (9/10), 1099–1124.
Mariani, S., Uriz, M.-J., Turon, X., 2000. Larval bloom of the oviparous sponge *Clionia viridis*: coupling of larval abundance and adult distribution. Mar. Biol. 137, 783–790.
Marshall, C., Javaux, E.J., Knoll, A.H., Walter, M., 2005. Combined micro-Fourier transform infrared (FTIR) spectroscopy and micro-Raman spectroscopy of Proterozoic acritarchs: a new approach to Palaeobiology. Precambr. Res. 138 (3–4), 208–224. https://doi.org/10.1130/B25892.1.
Marshall, A.O., Marshall, C.P., 2015. Vibrational spectroscopy of fossils. Paleontology 58 (2), 201–211. https://doi.org/10.1111/pala.12144.
Martin, D., Briggs, D.E.G., Parkes, R.J., 2003. Experimental mineralization of invertebrate eggs and the preservation of Neoproterozoic embryos. Geology 31 (1), 39–42.
Martin, D., Briggs, D.E., Parkes, R.J., 2004. Experimental attachment of sediment particles to invertebrate eggs and the preservation of soft-bodied fossils. J. Geol. Soc. 161 (5), 735–738.
Martin, D., Briggs, D.E.G., Parkes, R.J., 2005. Decay and Mineralization of Invertebrates eggs. Palaios 20, 562–572. https://doi.org/10.2110/palo.2004.p04-67.
McLaren, I.A., 1965. Some relationships between temperature and egg size, body size, development rate, and fecundity, of the copepod *Pseudocalanus*. Limnol. Oceanogr. 10 (4), 528–538.
Mélida, H., Sandoval-Sierra, J.V., Diéguez-Uribeondo, J., Bulone, V., 2013. Analyses of extracellular carbohydrates in oomycetes unveil the existence of three different cell wall types. Eukaryot. Cell 12 (2), 194–203.
Mertens, J., Beladjal, L., Alcantra, A., Fougnies, L., Van Der Straeten, D., Cleg, J., 2008. Survival of dried eukaryotes (anhydrobiotes) after exposure to very high temperatures. Biol. J. Linn. Soc. 93, 15–22.
Mills, D.B., Francis, W.R., Canfield, D.E., 2018. Animal origins and the Tonian Earth system. Emerging Topics in Life Sciences, ETLS20170160.
Mills, C.E., Strathman, M.F., 1992. Chapter 5: Phyllum Cnidaria, Class Hydrozoa. In: Strathman, M.F. (Ed.), Reproduction and development of Marine Invertebrates of the Northern Pacific Coast. Data and methods for the study of Eggs, Embryos, and Larvae. University of Washington Press, pp. 682.
Mills, D.B., Francis, W.R., Vargas, S., Larsen, M., Elemans, C.P., Canfield, D.E., Wörheide, G., 2018b. The last common ancestor of animals lacked the HIF pathway and respired in low-oxygen environments. Elife 7, e31176.
Moczydlowska, M., 2016. Algal affinities of Ediacaran and Cambrian organic walled microfossils with internal reproductive bodies: *Tanarium* and other morphotypes. Palynology 40 (1), 83–121.
Moczydlowska, M., Willman, S., 2009. Ultrastructure of cell walls in ancient microfossils as a proxy to their biological affinities. Precambr. Res. 173, 27–38. https://doi.org/10.1016/j.precamres.2009.02.006.
Moczydlowska, M., Schopf, W.J., Willman, S., 2010. Micro- and nano-scale ultrastructure of cell walls in Cryogenian microfossils: revealing their biological affinity. Lethaia 43, 129–136. https://doi.org/10.1111/j.1502-3931.2009.00175.x.
Moestrup, Ø., Inouye, I., Hori, T., 2003. Ultrastructural studies on Cymbomonas tetramitiformis (Prasinophyceae). I. General structure, scale microstructure and ontogeny. Can. J. Bot. 81 (7), 657–671.
AMory, A.J., Haines, P.W., (editors), 2005. GSWA Lancer 1 well completion report (interpretive papers), Officer and Gunbarrel Basins, Western Australia: Western Australia. Geological Survey, Record 2005/4, p. 81.
Mura, G., 2001. Morphological diversity of the resting eggs in the anostracean genus *Chirocephalus* (Crustacea, Branchopodia). Hydrobiologia 450, 173–185.
Muzzarelli, R.A.A., 1977. Chitin. Pergamon Press, New York.
Myers, J., Shaw, R., Tyler, I., 1996. Tectonic evolution of Proterozoic Australia. Tectonics 15 (6), 1431–1446.
Nagovitsin, K.E., Rogov, V.I., Marusina, V.V., Karlova, G.A., Kolesnikov, A.V., Bykova, N.V., Grazhdankin, D.V., 2015. Revised Neoproterozoic and Teereneuvian stratigraphy of the Lena-Anabar Basin and north-western slope of the Olenek Uplift, Siberian Platform. Precambr. Res. 270, 226–245.
Osinga, R., Tramper, J., Wijffels, R.H., 1999. Cultivation of Maine Sponges. Mar. Biotechnol. 1, 509–532.
Pan, Y., Wang, Y., Sha, J., Liao, H., 2015. Exceptional preservation of clam shrimp (Branchiopode, Eucrustacea) eggs from the Early Cretaceous Jehol Biota and implications for paleoecology and taphonomy. J. Paleontol. 89 (3), 369–376.
Pandey, K.K., 1999. A study of Chemical Structure of soft and hardwood and wood polymers by FTIR spectroscopy. J. Appl. Polym. Sci. 71, 1969–1975.
Parfrey, L.W., Lahr, D.J.G., Knoll, A.H., Katz, L.A., 2011. Estimating the timing of early eukaryotic diversification with multigene molecular clocks. PNAS 108 (33), 13624–13629.
Peng, Y., Bao, H., Yuan, X., 2009. New morphological observations for Paleoproterozoic acritarchs from the Chuanlinggou Formation, North China. Precambr. Res. 168 (3–4), 223–232.
Piraino, S., 1992. The "stinging" egg of *Clavopsella michaeli* (Berrill) (Hydrozoa, Cnidaria). Italian J. Zool. 59 (3), 251–256.
Pisani, D., Poling, L.L., Lyons-Weiler, M., Hedges, S.B., 2004. The colonization of land by animals: molecular phylogeny and divergence times among the arthropods. BMC Biol. 2 (1), 1. https://doi.org/10.1186/1741-7007-2-1.
Porter, S.M., 2016. Tiny vampires in ancient seas: Evidence for predation via perforation in fossils from the 780–740 million-year-old Chuar Group, Grand Canyon, USA. Proceedings of the Royal Society B: Biological Sciences 283, 1831.
Porter, S.M., Riedman, L.A., 2019. Evolution: Ancient Fossilized Amoebae Find Their Home in the Tree. Curr. Biol. 29 (6), 212–215.
Porter, S.M., Meisterfeld, R., Knoll, A.H., 2003. Vase-shaped microfossils from the Neoproterozoic Chuar Group, Grand Canyon: a classification guided by modern testate amoebae. J. Paleontol. 77, 409–429.
Porter, S. M., Agić, H., Riedman, L. A., 2018. Anoxic ecosystems and early eukaryotes. Emerging Topics in Life Sciences, ETLS20170162.
Preiss, W.V., 2000. The Adelaide Geosyncline of South Australia and its significance in Neoproterozoic continental reconstruction. Precambr. Res. 100, 21–63.
Pueschel, C.M., Sullivan, K., Ballantine, D.L., 1997. Ultrastructure of *Verdigellas peltata* (Palmellaceae, Chlorophyta), a deep-water, palmelloid alga with ferritin and trilaminar sheaths. Phycologia 36 (6), 492–499.
Pyle, L.J., Narbonne, G.M., Nowlan, G.S., Xiao, S., James, N.P., 2006. Early Cambrian metazoan eggs, embryos and phosphatic microfossils from Nothwestern Canada. J. Paleontol. 80 (5), 811–825.
Raff, E.C., Villinski, J.T., Turner, F.R., Donoghue, C.J., Raff, R.A., 2006. Experimental taphonomy shows the feasibility of fossil embryos. PNAS 103 (15), 5846–5851.
Riedman, L.A., Sadler, P.M., 2017. Global species richness record and biostratigraphic potential of early to middle Neoproterozoic eukaryote fossils. Precambr. Res. 319, 6–18.
Riedman, L.A., Porter, S.M., Halverson, G.P., Hurtgen, M.T., Junium, C.K., 2014. Organic-walled microfossil assemblages from glacial and interglacial Neoproterozoic units of Australia and Svalbard. Geology 42 (11), 1011–1014. https://doi.org/10.1130/G35901.1.
Riesgo, A., Maldonado, M., 2009. Ultrastructure of oogenesis of two oviparous demosponges, Axinella damicornis and Raspaciona acuelata (Porifera). Tissue Cell 41, 51–65.
Santella, L., Ianora, A., 1990. Subitaneous and diapause eggs in Mediterranean populations of *Pontella mediterranea* (Copepoda: Calanoida): a morphological study *. Mar. Biol. 105, 83–90.
Samchyshyna, L., Santer, B., 2010. Chorion structure of diapause and subitaneous eggs of four diaptomid copepods (*Calanoida,* Diaptomidae): SEM observations. Vestnik zoologii 44 (3), 26–32.
Sauerer, B., Craddock, P.R., Aljohani, M.D., Alsamadony, K.L., Abdallah, W., 2017. Fast and accurate shale maturity determination by Raman spectroscopy measurement with minimal sample preparation. Int. J. Coal Geol. 173, 150–157. https://doi.org/10.1016/j.coal.2017.02.008.
Schopf, J.W., Kudryavtsev, A.B., Agresti, D.G., Czaja, A.D., Wdowiak, T.J., 2005. Raman imagery: a new approach to assess the geochemical maturity and biogenicity of permineralized Precambrian fossils. Astrobiology 5 (3), 333–371.
Scholz, M.J., Weiss, T.L., Jinkerson, R.E., Jing, J., Roth, R., Goodenough, U., Posewitz, M.C., Gerkene, H.G., 2014. Ultrastructure and composition of the Nannochloropsis gaditana Cell Wall. Eukaryot. Cell 13 (11), 1450–1464.
Schwelm, A., Fogelqvist, J., Knaust, A., Jülke, S., Lilja, T., Bonilla-Rosso, G., Karlssons, M., Shevchenko, A., Dhandapani, V., Choi, S.R., Kim, H.G., Park, J.Y., Lim, Y.P., Ludwig-Müller, J., Dixelius, C., 2015. The Plasmodiophora brassicae genome reveals insights on its life cycle and ancestry of chitin synthases. Sci. Rep. 5, 11153.
Sergeev, V.N., Schopf, J.W., 2010. Taxonomy, paleoecology and biostratigraphy of the

late Neoproterozoic Chichkan microbiota of south Kazakhstan: the marine biosphere on the eve of metazoan radiation. J. Paleontol. 84 (3), 363–401.
Shaeder, M., 1996. Factors influencing egg size in the gammarid amphipod *Gammarus insensibilis*. Mar. Biol. 124, 519–526.
Shields-Zhou, G.A., Porter, S., Halverson, G.P., 2016. A new rock-based definition for the Cryogenian Period (circa 720–635 Ma). Episodes 39 (3), 3–8.
Simpson, T.L., 1984. The cell biology of sponges. Springer-Verlag, New York Inc.
Stevens, M.K., Apak, S.N., (compilers), 1999. GSWA Empress 1 and 1A well completion report, Yowalga Sub-basin, Officer Basin, Western Australia. Western Australia Geological Survey, Record 1999/4 110.
Straathof, G.B., 2011. Neoproterozoic low latitude glaciations: an African perspective. University of Edimbourgh.
Strathman, M.F., 1992. Chapter 4: Phyllum Cnidaria, Class Anthozoa. In: Strathman, M.F. (Ed.), Reproduction and development of Marine Invertebrates of the Northern Pacific Coast. Data and methods for the study of Eggs, Embryos, and Larvae. University of Washington Press, pp. 682.
Swanson-Hyssel, N.L., Maloof, A.C., Condon, D.J., Jenkin, G.R.T., Alene, M., Tremblay, M.M., Tesema, T., Rooney, A.D., Haileab, B., 2015. Stratigraphy and geochronology of the Tambien Group, Ethiopa: Evidence for globally synchronous carbon isotope change in the Neoproterozoic. Geology 43 (4), 323–326. https://doi.org/10.1130/G36347.1.
Tack, L., Wingate, M.T.D., Liégois, J.-P., Fernandez-Alonso, M., Deblond, A., 2001. Early Neoproterozoic magmatism (1000–910 Ma) of the Zadinian and Mayumbian Groups (Bas-Congo): onset of Rodinia rifting at the western edge of the Congo craton. Precambr. Res. 110, 277–306.
Tait, J., Delpomdor, F., Préat, A., Tack, L., Straathof, G., Kanda Nkula, V., 2011. Neoproterozoic sequences of the West Congo and Lindi/Ubangi Supergroups in the Congo Craton, Central Africa. In: E. Arnaud, G. Halverson. G.A. Shields (Eds), The Geological Record of Neoproterozoic glaciations. Geological Society of London, Memoir 36, 185-1994.
Tang, Q., Pang, K., Yuan, X., Wan, B., Xiao, S., 2015. Organic-walled microfossils from the Tonian Gouhou Formation, Huaibei region, North China Craton, and their biostratigraphic implications. Precambr. Res. 266, 296–318.
Talyzina, N.M., Moczydlowska, M., 2000. Morphological and ultrastructural studies of some acriatrchs from the lower Cambrian Lükati Formation, Estonia. Rev. Palaeobot. Palynol. 112, 1–21.
Thiéblemont, D., Castaing, C., Billa, M., Bouton, P., Préat, A., 2009. Notice explicative de la Carte géologique et des Ressources minérales de la République gabonaise à 1/1 000 000. Editions DGMG, Ministère des Mines, du Pétrole, des Hydrocarbures. Libreville.
Timmons, J.M., Karlstrom, K.E., Dehler, C.M., Geissman, J.W., Heizler, M.T., 2001. Proterozoic multistage (~1.1 and ~0.8 Ga) extension in the Grand Canyon Supergroup and vestablishment of northwest and north-south tectonic grains in the southwestern United States. Geol. Soc. Am. Bull. 113, 163–180.
Van Bergen, P.F., Blokker, P., Collinson, M.E., Sinninghe Damsté, J.S., de Leeuw, J.W., 2004. 8: Structural biomacromolecules in plants: what can be learnt from the fossil record? In: Hemsley, A.R., Poole, I. (Eds.), The evolution of plant physiology. Evolution of plant physiology. Elsevier, Amsterdam.
Van Waveren, I.M., 1993. Planktonic organic matter in surficial sediments of the Banda Sea (Indonesia) - a palynological approach. Geol. Ultraiect. 104, 237 p.
Versteegh, G.J.M., Blokker, P., 2004. Resistant macromolecules of extant and fossil microalgae. Phycol. Res. 52, 325–339.
Versteegh, G.J.M., Blokker, P., Marshall, C., Pross, J., 2007. Macromolecular composition of the dinoflagellate cyst *Thalassiphora pelagic* (Oligocene, SW Germany). Org Geochem. 38, 1643–1656.
Versteegh, G.J.M., Blokker, P., Bogus, K.A., Harding, I.C., Lewis, J., Oltmanns, S., Rochon, A., Zonneveld, K.A.F., 2012. Infrared spectroscopy, flash pyrolysis, thermally assisted hydrolysis and methylation (THM) in the presence of tetramethylammonium hydroxide (TMAH) of cultured and sediment-derived Lingulodinium polyedrum (Dinoflagellata) cyst walls. Org Geochem. 43, 92–102.
Wall, D., 1962. Evidence from Recent plankton regarding the biological affinities of Tasmanites Newton 1875 and Leiosphaeridia Eisenack 1958. Geol. Mag. 99, 353–362.
Walter, M., Veevers, J., Calver, C., Grey, K., 1995. Neoproterozoic stratigraphy of the Centralian Superbasin, Australia. Precambr. Res. 73, 173–195.
Wang, S., Sun, S., 2007. Comparative observation on the cyst shells of seven *Artemia* strain from China. Microsc. Res. Tech. 70, 663–670.
Wanjun, T., Cunxin, W., Doughua, C., 2005. Kinetic studies on the pyrolysis of chitin and chitosan. Polym. Degrad. Stab. 87 (3), 389–394.
Watanabe, M., 2006. Anhydrobiosis in invertebrates. Appl. Entomol. Zool. 41 (1), 15–31.
Willman, S., 2009. Morphology and wall ultrastructure of leiosphaeric and acanthomorphic acritarchs from the Ediacaran of Australia. Geobiology 7, 8–20. https://doi.org/10.1111/j.1472-4669.2008.00178.x.
Willman, S., Moczydlowska, M., 2007. Wall ultrastructure of an Ediacaran acritarch from the Officer Basin, Australia. Lethaia 40, 111–123. https://doi.org/10.1111/j.1502-3931.2007.00023.x.
Willman, S., Cohen, P.A., 2011. Chapter 12: Ultrastructural Approaches to the Microfossil Record: Assessing Biological Affinities by Use of Transmission Electron Microscopy. In: Laflamme, M., Schiffbauer, J.D., Dornbos, S.Q. (Eds.), Quantifying the evolution of Early Life, Numerical approach to the evaluation of Fossils and ancient ecosystems, Springer, Topics in Geobilogy 36, pp. 462.
Wood, R., Erwin, D.H., 2018. Innovation not recovery: dynamic redox promotes metazoan radiations. Biol. Rev. 93 (2), 863–873.
Wysokowki, M., Zaton, M., Bazhenov, V.V., Behm, T., Ehrlich, A., Stelling, A.L., Hog, M., Ehrlich, H., 2014. Identification of chitin in 200-million-year-old gastropod egg capsules. Paleobiology 40 (4), 529–540.
Xiao, S., 2002. Mitotic topologies and mechanisms of Neoproterozoic algae and animal embryos. Paleobiology 28 (2), 244–250.
Xiao, S., Knoll, A.H., 2000. Phosphtized animal embryos from the Neoproterozoic Doushantuo Formation at Weng'an, Guizhou, South China. J. Paleontol. 74 (5), 767–788.
Xiao, S., Schiffbauer, J.D., 2009. Microfossil Phosphatization and Its Astrobiological Implications. In: In: Seckbach, J., Walsh, M. (Eds.), From Fossils to Astrobiology. Cellular Origin, Life in Extreme Habitats and Astrobiology, vol 12 Springer, Dordrecht.
Xiao, S., Tang, Q., 2018. After the boring billion and before the freezing millions: evolutionary patterns and innovations in the Tonian Period. Emerging Topics Life Sci ETLS20170165.
Xiao, S., Hagadorn, J.W., Zhou, C., Yuan, X., 2007. Rare helical spheroidal fossils from the Doushantuo Lagerstätte: Ediacaran animal embryos come of age? Geology 35 (2), 115–118.
Yan-bin, S., Di-ying, H., 2008. Extant clam shrimp egg morphology: taxonomy and comparison with other fossil branchiopod eggs. J. Crustac. Biol. 28 (2), 352–360.
Yang, E.C., Boo, S.M., Bhattacharya, D., Saunders, G.W., Knoll, A.H., Fredericq, S., Graf, L., Yoon, H.S., 2016. Divergence time estimates and the evolution of major lineages in the florideophyte red algae. Sci. Rep. 6, 1–11.
Yin, L.M., Zhou, C.M., Yuan, X.L., 2008. New data on *Tianzhushania,* an Ediacaran diapauses egg cyst from Yichang, Hubei. Acta Paleontologica Sinica 47 (2), 129–140.
Zang, W.L., Walter, M.R., 1992. Late Proterozoic and early Cambrian microfossils and biostratigraphy, northern Anhui and Jiangsu, central-eastern China. Precambr. Res. 57, 243–323.
Zhang, Y., Zhang, X., 2017. New *Megasphaera*-like microfossils reveal their reproductive strategies. Precambr. Res. 300, 141–150.
Zhou, C., Tucker, R., Xiao, S., Peng, Z., Yuan, X., Chen, Z., 2004. New constraints on the age of Neoproterozoic glaciation in south China. Geology 32 (5), 447–1430. https://doi.org/10.1130/G20286.
Zumberge, J.A., Love, G.D., Cárdenas, P., Sperling, E.A., Gunasekera, S., Rohrssen, M., Grosjean, E., Grotzinger, J.P., Summons, R.E., 2018. Desmosponge steroid biomarker 26-methylstigmastane provides evidences for Neoproterozoic animals. Nat. Ecol. Evol. 2, 1709–1714.
Ogurtsova, R.N., Sergeev, V.N., 1989. Megasferomorfidy Chichkanskoi svity verkhnego Dokembriia iuzhnogo Kazakhstana [Megaspheromorphids from the upper Precambrian Chichkan Formation, southern Kazakhstan]. *Paleontologicheskii Zhurnal 2 [Paleontological Journal 2]*, 119-122 [in Russian].